The Functional Morphology of Hard-Prey Crushing Teeth

Stephanie B. Crofts

A dissertation

submitted in partial fulfillment of the

requirements for the degree of

Doctor of Philosophy

University of Washington

2015

Reading Committee:

Adam Summers, Chair

Christian Sidor

Greg Wilson

Program Authorized to Offer Degree:

Department of Biology

University of Washington

Abstract

The Functional Morphology of Hard-Prey Crushing Teeth

Stephanie B. Crofts

Chair of the Supervisory Committee:
Professor Adam Summers
Department of Biology

Durophagy is the consumption of hard-shelled prey-items, like shelled molluscs and crustaceans with hard exoskeletons. In order to break these hard shells, organisms need to be able to generate large bite-forces, which are transferred to the prey via the teeth. As such, the teeth of durophagous predators are specialized, and are typically described as "flattened," "molariform," "pavement-like," "pebble-like," or "hemispherical." But these descriptors do not accurately reflect the diversity of tooth morphologies seen in hard-prey specialists. Teeth can vary in occlusal convexity from highly domed to flat, but may also be concave, and some even have small cusps, presumably to concentrate stress applied to their prey. This variation in morphology indicates that there should also be variation in tooth function, but little experimental work has been done on the function of durophagous teeth.

The goals of this thesis are fourfold: 1) To use canonical models of durophagous teeth to test how much force different occlusal morphologies require to break prey items; 2) To use finite element models of the same set of canonical teeth to test how these different morphologies are able to disperse and distribute in-tooth strain and resist failure; 3) To use these two studies to identify functional trade-offs and predict a theoretical optimal tooth; 4) To use the extinct clade of marine reptiles, the Placodontia, as a case study to see if functional trade-offs can allow us to predict durophagous tooth morphologies, and to determine what other factors may be in play.

TABLE OF CONTENTS

LIST OF FIGURES

LIST OF TABLES

ACKNOWLEDGEMENTS

This research would not have been possible without the help and contributions from a huge number of people.

Huge thanks go to A. P. Summers, a great advisor who helped me to learn how to ask interesting questions and communicate results, and who always had my back. Thank you as well to G. Wilson and C. Sidor who helped me refine my questions and who welcomed me into the Seattle Paleo Group. Thanks to T. Popowics for being a cheerful and supportive GSR at every step of the way.

Thanks also to J. Brash and the FHL Maintenance Crew, who not only taught me how to machine parts, but always had a smile and a kind word while I was working at the CNC Mill. Thanks also to T. Kleinteich (and family), specifically for his work scanning, sectioning, and futzing about with snail scans, and more generally for being a great lab member. Thanks also to T. Cox and R. Shahar for their help with the shells, and E. Carrington and M. Dethier for providing the initial shells. Thanks to T. Daniel for getting me started down the FEA path, P. Reinhall, B. Dumont, and I. Grosse for setting me straight when I erred, and A. Erlebe for being a sounding board for ideas and general source of FEA advice.

I have met too many people at FHL through the years to be able to sufficiently thank them all. The administrators and staff have been an amazingly supportive community, and I can't imagine my time at the labs without them. Thanks also to the great classes that I've been involved with at the labs, the Fish class of 2010, where the first ideas of the dissertation sparked, and the Invert class of 2013 and Fish class of 2014, both of which allowed me to work with some amazing researchers. Thanks also to J. Grewal, V. Hoang, and A. Vanci, for their enthusiasm and dedication to crushing shells, and to L. Brandkamp, T. Huang, and K. Bigham, for their work with the crabs. Thanks especially to J. Lomax for being a joy to work with and making the crushing question his own. I especially have to thank the fantastic community of grad students, lab techs, divers, staff, visiting researchers, etc. who made the island a home.

I also have to thank all the people in Seattle who helped me find my place on main campus: the denizens of the "Biohouse" over the years, the Seattle Bio department, and especially the Paleo work group. Thanks also to Mandy Schivell, who taught me so much about how to teach, and has been a great friend and mentor. I would have been lost without M. J. Heringer, J. Farrow, and S. O'Hara and all their help navigating the administrative aspects of the department. Finally, a huge thanks to T. Bradshaw and J. Tewksbury for their time and encouragement.

I would have been literally and figuratively lost when measuring Placodont skulls if it weren't for the help of a huge number of curators and researchers throughout Europe, as well as their work groups. Thank you so very much P. Havlik, B. Herkner, G. Köhler, G. Muscio, J. Neenan, D. C. Nieweg, S. Nosotti, C. Dal Sasso, T. Scheyer, R. Schoch, D. Schwarz-Wings, as well as the other graduate students, post-docs, undergrads, and researchers who helped me and made me feel so welcome. Thanks also to the various institutions that hosted me and allowed me access to their collections: Museum für Naturkunde, Berlin; TwentseWelle, Enschede; Staatliches Museum für Naturkunde, Stuttgart ; Senckenberg Center for Human Evolution and Palaeoenvironment, Tübingen; Senckenberg Forschungsinstitut und Naturmuseum; Paläontologisches Institut und Museum, Zurich; Museo Civico di Storia di Milano; Museo Friulane di Storia Naturale, Udine. Thanks also to P. Falkingham for introducing me to photogrammetry, and for all the help when I tried it for myself.

Thank you to the members of the Summers lab, and my collaborators over the years. Thanks to M. Porter, M. Dean, A. Clark, and J. Horton for welcoming me to the Summers lab oh so long ago and far away, and thanks to M. Paig-Tran, who made the move to Seattle with me - I couldn't ask for a better academic sister. Thanks to J. Bizarro for being a great labmate and helping me learn how to ID flatfishes. Thanks as well to the great Summers lab post-docs over the years: T. Kleinteich, A. Kleinteich, and P. Ditsche, and thanks to the many undergraduates and interns who have helped out around the lab over the years. Thanks to K. Dobkowski for being a great friend and I look forward to measuring all the kelp.

And finally, I can't thank my family enough, for all of their encouragement, patience, and understanding over the course of my graduate studies, especially for sitting through practice

SICB talks every winter break. Thank you especially to my parents for always encouraging my love of dinosaurs, and science in general.

Chapter 1. HOW TO BEST SMASH A SNAIL - THE EFFECT OF TOOTH SHAPE ON CRUSHING LOAD.

Crofts, S. B., and Summers, A. P. (2014). How to best smash a snail: the effect of tooth shape on crushing load. *J R Soc Interface* 11, 20131053.

Organisms that are durophagous, hard-prey consumers, have a diversity of tooth forms. To determine why we see this variation, we tested whether some tooth forms break shells better than others. We measured the force needed with three series of aluminium tooth models, which varied in concavity and the morphology of a stress concentrating cusp, to break a shell. We created functionally identical copies of two intertidal snail shells: the thicker shelled *Nucella ostrina* and the more ornamented *N. lamellosa* using a 3D printer. In this way, we reduced variation in material properties between test shells, allowing us to test only the interaction of the experimental teeth with the two shell morphologies. We found that for all tooth shapes, thicker shells are harder to break than the thinner shells and that increased ornamentation has no discernible effect. Our results show that for both shell morphologies, domed and flat teeth break shells better than cupped teeth, and teeth with tall or skinny cusps break shells best. While our results indicate that there is an ideal tooth form for shell breaking, we do not see this shape in nature. This suggests a probable trade-off between tooth function and the structural integrity of the tooth.

Key words: durophagy, tooth morphology, shell-failure, rapid-prototyping, biomechanics

1.1 INTRODUCTION

Teeth play an important role in the capture and processing of prey so it is not surprising that tooth morphology is closely correlated with diet. This relationship between tooth form and function is so strong that it is used to make inferences about the natural history of organisms. For example, Massare (1978) used the observed relationships between the tooth morphologies and diets of marine mammals to define and infer feeding guilds of extinct marine reptiles. The broadest categories, which could be combined to generate additional guilds, consisted of: hard prey crushing organisms, organisms with piercing teeth to eat soft invertebrate prey, and organisms with bladed teeth to cut through the flesh of large vertebrate prey. While these guilds are based on observed correlations between morphology and consumed prey, they do not explain why some morphologies are better at processing some prey items than others.

Models, both physical and mathematical, have been used to test tooth shapes associated with different feeding guilds. Based on observed tooth morphologies and general engineering principles, Evans and Sanson (2003; 2006) generated "ideal" cutting teeth. These theoretical teeth broadly reflected a diversity of mammalian teeth, both extinct and extant. In a more experimental context, the morphology of notched blades has been demonstrated to have a significant effect on the ease with which tough prey items are cut (Anderson, 2009; Anderson and LaBarbera, 2008). Similarly, the functional advantages of serrated teeth have been demonstrated when tearing through muscle (Abler, 1992). The function of puncturing teeth has also been explored using models that varied in aspect ratio and taper, in order to compare bite-forces and how different morphologies bend (Freeman and Lemen, 2007). Physical models have also been employed to better understand how puncture and cutting performance differ between different extant and extinct shark tooth morphologies (Whitenack and Motta, 2010).

There has been some physical modelling of the performance of specific hard prey crushing dentitions -- Schulp (2005) used replicas of the crushing teeth of the mosasaur, *Carinodens belgicus* to break potential prey items. By comparing the force needed to break the prey items with bite forces calculated based on jaw morphology, he demonstrated that soft bodied prey, such as squid, were unlikely prey items for *C. belgicus*, and that hard bodied organisms, such as sea urchins, arthropods, bivalves and gastropods were more likely prey. However the ability of the teeth to process hard shelled prey very much depended on the shell thickness and

morphology, as well as where forces were applied. While this study nicely demonstrated the functional limitations of a single crushing tooth morphology it does not explain the morphology of the *C. belgicus* crushing teeth, or why they were able to process some prey items, like whelk snails but not others, like winkle snails.

The literature of durophagy focuses on the defensive adaptations of the prey rather than the morphology of the crushing apparatus. Though this dentition is readily recognized in extant and fossil taxa, the precise morphology is variable and the implications of shape on performance are not understood. The teeth of durophagous organisms have been described as "flattened", "pavement-like", "molariform", and "pebble-like" (Mara et al., 2010; Mehta, 2009; Sasko et al., 2006; Summers, 2000; Wilga and Motta, 2000). These terms lack precision and do not cover the diversity of morphologies seen in the hard prey crushing teeth of durophagous animals (Fig. 1.1). Crushing teeth can range from domed, to flat plates, and can be worn to the point of concavity. Additionally, durophagous teeth can have a range of different cusp morphologies which serve to concentrate forces and increase stress on the prey item.

The goals of this study are four-fold: 1) establish that rapid prototyping and computer numerical control (CNC) milling can be used to generate repeatable performance data on crushing load by standardizing both tooth shape and prey morphology; 2) determine the effect of crown concavity/convexity on the load needed to fracture prey; 3) quantify the role of a centrally located stress concentrator on breaking load; 4) determine whether the optimal tooth shape is sensitive to subtle variations in the prey morphology. We can then use these results to discuss the implications of some extant and extinct crushing dentitions.

1.2 MATERIALS AND METHODS

1.2.1 *Tooth Models*

To isolate and test the performance of different aspects of tooth morphology we created three series of models spanning a range of morphologies to reflect tooth morphologies seen in nature, as well as extreme morphologies. Model shapes were generated by rotating a section, from $x = 0$ to $x = 1$, of a parametric curve (eq. 1.1) about its y-axis.

$$y = -(x^{32} - h \times exp^{-(\frac{x^2}{r})})$$

(1.1)

We varied different aspects of model morphology by changing two parameters: *h*, which controls the height of cusps projecting from the occlusal surface, and *r*, which controls how much of the occlusal surface the base of a projecting cusp covers. By setting *h* and *r* parameters to zero, we generated a tooth model with a flat occlusal surface, which we considered the ground state (model 0). Our first series consisted of 5 tooth models whose occlusal surface ranged from concave to convex (Fig. 1.2a). We achieved this by setting *r* approximately equal to the radius of the occlusal surface ($r = 0.4$) and then varied *h* from 0.5 to -0.5. For the second series we compared model 0 to five models with central occlusal cusps of varying height (Fig. 1.2b). To create a small cusp in the middle of the occlusal surface we set $r = 0.1$ and then varied the cusp height by changing *h* from 0.1 to 0.5. In our third set of tooth models, we varied the occlusal area covered by the base of a cusp of constant height (Fig. 1.2c). To do this, cusp height (*h*) was set to 0.25, and the width of the cusp base was varied from $r = 0.35$ to $r = 0$ (model 0). Milling tool paths were created from the model geometry with SprutCAM 7.0 and milled from round aluminium stock (6061 T6) on a Tormach mill with a 0.082 round carbide endmill. The end result are tooth models with bodies approximately 12.5mm in diameter, with a Young's modulus of 68.9GPa, which is lower than the Young's modulus reported for human enamel (Lucas et al., 2008) or shark enameloid (Whitenack et al, 2010).

1.2.2 *Shell Copies*

Because we were interested in testing only the effects of tooth morphology on crushing ability, we mass produced shells for testing using a rapid prototyper (ZPrinter 310,

ZCorporation). This eliminated variation in shell material properties due to the natural history of the individual and variation in covarying aspects of morphology. For example, opercular width is correlated with length but is not invariant with length. By printing the same shell multiple times we ensured the exact same gross morphology. This leaves variation in microscale morphology, such as distributions of microfractures and inclusions that dictate the stochastic nature of failure. We tested two shell morphologies, based on data from CT scans of intertidal gastropods (collected at Friday Harbor Labs, WA) *Nucella ostrina* (Fig. 1.3a) and *N. lamellosa* (Fig. 1.3b), each demonstrating various adaptations to prevent crushing. By using CT data, we were able to accurately replicate the entire internal and external morphology of both shells in our copies. The relatively shorter spire in the *N. ostrina* specimen should be less prone to cracking, while the more developed ornamentation on *N. lamellosa* may provide increased structural support (Vermeij, 1977). The *N. ostrina* also has thicker body whorl walls, which would make the shell sturdier. Surface data from each shell were generated from microCT scans and rendered in Amira (version 5.2.2), then uploaded and scaled so that the shell height of each measured 25mm (ZPrint version 7.10.3-7). We printed shell replicas using zp150 high performance composite powder and zb60 binding solution, and then hardened them with a misting of a saturated Epsom salt solution. In this way we were able to generate two morphologically distinct sets of shell copies that behaved as brittle solids (Fig. 1.4a) with effectively identical material properties: a Young's modulus of 314.977 ± 32.49 (MPa) and compressive strength 4.54 ± .0.76 (MPa). In contrast to real mollusc shells, our models lack a complicated microstructure, which function to confound crack propagation in living molluscs. However, for the purposes of this study, we are focusing only on the force needed to initiate crack formation, not propagate it.

To determine that the rapid prototyper produced shells that would fail reproducibly, we printed and tested small batches of shells. To measure the force needed to break the shells, we attached the flat tooth model (model 0) to a moving 500N load cell in a materials testing system (MTS; Synergie 100, MTS Systems Corporation), directly over a printed shell placed aperture down. The shells were positioned so that the tallest point of the body whorl was centred under the tooth model, and were placed on a 5mm, 60 durometer silicone rubber pad to reduce stress concentrations in the printed shell due to interactions between the shell and platform. The tooth model was lowered directly onto the printed shell at a rate of 1.27 mm/min. We found no difference between initial load to failure for shells from different batches (t-test; $n = 5$; $p = 0.80271$), so long as they were allowed to dry and set for at least one day before testing.

For both shell morphologies, fractures occurred in the main body whorl, at the point of loading and radiated out. The point at which crack initiation occurred was ~ 1.4 mm thick in *N. lamellosa*, and ~ 2.25 mm thick in *N. ostrina*. Cracks most often propagated around the circumference of the shell. Occasionally cracks would also travel along the long axis of the shell, moving towards the siphonal notch (Fig. 1.4b &c). As a result of testing, shells were completely destroyed, as described by Zushcin *et al.* (2003), and as would be expected from crushing predators.

1.2.3 *Tests and Analysis*

Testing the various combinations of different tooth models and shell morphologies followed the same procedure as the batch testing. For each tooth model/shell combination, we tested 25 shells and measured the initial load of failure (F in N), defined as the first point at which the load dropped by 60% (Fig. 1.4a). The initial load of failure is an indicator of how

much energy the predator needs to expend to break shells of different morphology, but the same size.

Since the shells had different morphologies and were quite different in shell thickness, we also calculated the force to initiate crack propagation per unit volume (F/V in N/cm^3) of each shell by dividing the initial load of failure by the volume of material that was used to make the shell. *N. ostrina* was slightly more voluminous ($1.08cm^3$) than *N. lamellosa* ($0.83cm^3$), reflecting the difference in shell wall thickness. The difference in volume can reflect a difference in energy invested in generating the shell, so the force per volume measurement will allow us to see how different shell architecture interacts with different tooth morphologies.

Both sets of data were log transformed to achieve a normal distribution. The interactions between shell and tooth morphology were compared for all three series of tooth models with a 2-way ANOVA and post-hoc Tukey's tests in R.

1.3 RESULTS

Average results and standard deviations for all tests are given in Table 1. Across all tests, *Nucella lamellosa* required less force to initiate crack propagation than *N. ostrina*. The force to initiate crack propagation was significantly higher for *N. ostrina* shells than for *N. lamellosa* for all tooth models (2-way ANOVA: $F_{1,240}$=1333.42, P<<0.001) and the force normalized by volume followed a similar pattern for both shell morphs.

The force to failure normalized by shell volume for the first series of tooth models tested, where models varied by occlusal concavity and convexity, are illustrated in Figure 1.5a. In addition to the difference between the shells, there were also significant differences in the force needed to initiate crack propagation between tooth model morphologies (2-way ANOVA: $F_{4,240}$=292.76, P<<0.001), and significant interaction effects for the force measurements (2-way

ANOVA: $F_{4,240}$=73.91, P<<0.001). For *N. ostrina*, the two concave models (-2, -1) require significantly more force than the flat and two convex morphologies (0, 1, 2) to initiate crack propagation (P<<0.001). For *N. lamellosa*, in contrast, only the most concave tooth (-2) takes significantly more force (P<<0.001). Significant differences (2-way ANOVA: $F_{4,240}$=1128.5 , P<<0.001) and interaction effects 2-way ANOVA: $F_{4,240}$=400.8, P<<0.001) also existed when force of initial failure was normalized by volume; when adjusting for volume of shell material, all shell-tooth model interactions are significantly different (P<0.05), except for the flat (0) and most convex (2) tooth in *N. ostrina*, and the flat tooth (0) (P<0.05) and the shallow convex tooth (1) in *N. lamellosa*.

The effects of adding a stress concentrating cusp of varying heights on the force per volume needed to initiate crack propagation in both shell types is demonstrated in Figure 1.5b. For both shells, there is a general trend of decreasing load to initial failure as cusp height increases, though this is more obvious in *N. ostrina*, and these trends hold true for the force normalized by shell volume. There are significant differences (2-way ANOVA: $F_{5,288}$=85 , P<<0.001) between the force needed by the different models to initiate crack propagation, as well as a significant interaction effect (2-way ANOVA: $F_{5,288}$=16.03 , P<<0.001), as well as for the force normalized by shell volume (2-way ANOVA: $F_{5,288}$=85 , P<<0.001; 2-way ANOVA: $F_{5,288}$=16.03 , P<<0.001). In *N. ostrina*, for both datasets, there is no significant difference between the flat tooth and the shortest two cusps (models 0, H1, H2), they differ from model H3, and a group formed by the tallest two cusps (H4 & H5) (P<<0.01). For *N. lamellosa*, the flat tooth (model 0) took significantly more force to initiate failure as well as initial force per volume (P<<0.001) than any other tooth model to initiate crack propagation. There was no significant difference between the first four cusp heights (models H1-4), all of which required an

intermediate amount of force, as well as force normalized by volume, to initiate crack propagation, and the fifth cusp height (model H5) took significantly less ($P<<0.001$).

Similarly, the patterns of initial force per unit volume needed to initiate crack propagation by cusps that taper to different degrees are illustrated in Figure 1.5c. For both shell morphs, narrowing the cusp decreases the force as well as force normalized by shell volume needed to initiate crack propagation. For the force needed to initiate crack propagation in *N. ostrina*, the flat tooth and the widest cusp (models 0 and R1) formed a significantly distinct group ($P<.01$), as did models R2 and R3 ($P<<0.01$), and R3 and R4 ($P<0.05$), with the narrowest model (model R5) being significantly different from any other model ($P <<0.001$). Similarly, for *N. lamellosa* the flat tooth model and the widest cusped model (models 0 and R1) were not statistically different from each other. All other models were significantly different ($P <0.05$), except models R1 and R3. There was a similar pattern for *N. lamellosa* when force to crack propagation was normalized by shell volume ($P>0.05$). For *N. ostrina*, however the pattern differed. The flat model and widest cups (models 0 and R1) still form a distinct group ($P<.01$), but model R1 is not statistically distinct form model R3. Finally, models R3 and R4 are not significantly different.

1.4 DISCUSSION

In cases such as this, investigating how changes in tooth and shell structures affect performance, rapid prototyping can be expedient in generating great quantities of experimental samples, while eliminating variation resulting from the natural history of the organism. The force needed to break mollusc shells can be highly variable, both within and between species (Zuschin and Stanton, 2001). This variation can be due to differences in gross morphology, such as shell thickness and ornamentation, well as microstructure, such as different shell composition and crystal orientation. This variability can make it difficult to ask specific morphological questions,

since one cannot control for all of these variables. With rapid prototyping, in contrast, you eliminate variation due to natural history and can replicate experiments using the same morphology, and control how morphology changes.

We tested two intertidal snail shell morphologies: the thick shelled, low spired *N. ostrina*, and the thinner shelled, high spired, and more ornamented *N. lamellosa*. Both shell types broke in a similar manner for all tooth model morphologies, with thicker shells requiring more force, even when normalized against the volume of the shell. The similarity in breaking pattern also indicates that having a taller shell spire does not affect the specifics of failure. However, this may be due to load placement on the shells, since tooth models were situated directly over the body whorl and were rarely in contact with the spire.

Concave teeth require more force to break shells than flat or convex teeth. This may be case dependent, however, since the body whorl of both shells fit into the concavity of the concave tooth models, which increased the area of the tooth in contact with the shell and decreased the applied stress. Similarly, the most convex tooth had the least surface area in contact with the shells, and in *N. lamellosa* trials took statistically less force to break than any other model in the series. While it was not significantly different, a similar pattern can be seen in the interaction between the most convex tooth and the *N. ostrina* shell.

Adding a cusp to the flat tooth concentrated the force being applied to the shell, and reduced the force needed to break both shell morphs. For both shell morphologies, there is a general pattern of decreasing force as cusp height increases. This trend is most distinct in *N. ostrina*, while in *N. lamellosa* there is very little difference in the force needed to break the shell for intermediate cusp heights. As with the cusp height, both shell morphs demonstrated a similar pattern of decreasing force per volume to break as cusps become narrower.

Based on these data, the most effective tooth for breaking shells is flat or convex with a tall skinny cusp. The closest tooth to this ideal in nature may be the snail punching sculpin *Asemichthys taylori* which uses teeth with a high central cusp on its vomer to punch small holes in snail shells before swallowing them whole (Norton, 1988). This shape will reduce the area being loaded and increase the stress on the shell for a given force, reducing the overall force needed to break the shell. Reducing the load needed to crush is clearly only part of the durophagy story though, because there are many different tooth morphologies in nature, and none fit this optimal shape. An explanation for the variation in tooth shape might in part be that not all hard prey is the same. Here we showed that even relatively small differences in snail shell shape can have an effect on how much force is needed to initiate crack propagation. Hard prey spans a wide range of organisms, from the well mineralized and brittle, like sea urchins and decapod crustaceans to tougher prey items, such as molluscs, which may reward different tooth shapes. Furthermore, it is intuitively clear that a high cusp is at greater risk of failure, so there is likely some trade-off between reducing the load needed to break the prey item and dissipating the load safely so the tooth does not fail.

In fact, different gnathostome lineages invest different amounts of energy when producing teeth. Some groups, such as sharks, create and regularly replace relatively simple teeth. Others, notably mammals, produce just a few sets of specialized teeth that are not replaced. This implies that the selective pressure to protect teeth from damage varies with phylogeny. The balancing act between damage to prey and tooth is well studied in mammals, especially those with bunodont dentition, such as humans or apes, where there is a wealth of literature on fracture mechanics. In these systems, enamel thickness and tooth size are aspects of the tooth that determine damage resistance, and food hardness is the prey's contribution to the damage

equation (Lucas et al., 2008; Berthaume et al., 2011; Lawn and Lee, 2009; Lee et al., 2011; Luke and Lucas, 1983; Lawn et al., 2013).

This trade-off between function and damage control should be of less importance in animals that frequently replace teeth, such as reptiles or fish (Lee et al., 2011). For example, the microstructure of tooth materials differs in non-mammals, with enamel crystals that are not arranged to deflect crack propagation (Sander, 2000). Lawn *et al.* extrapolate their findings to apply to sabre-toothed cats, as well as "crocodiles and many reptiles" with conical teeth (2013), so perhaps the puncturing case is well in hand. We suggest that looking at the stress distribution in crushing teeth would allow a direct measure of the risk of failure and, in a phylogenetic context, could be used to test the hypothesis that replacement rates affect risk tolerance in tooth design.

1.5 TABLES AND FIGURES

Figure 1.1 - Diversity of durophagous tooth morphologies. (a) *Placochelys placodonta* † MB.R. 1765 (b) *Dracaena sp.* (lizard) (c) *Rhina* (guitarfish) (d) *Anarrhichthys ocellatus* (wolf eel) (e) *Rhinoptera bonasus* (stingray) (f) *Acantholithodes hispidus* (hairy crab) (g) *Pugettia gracilis* (graceful kelp crab) (h) *Metacarcinus magister* (dungeness crab)

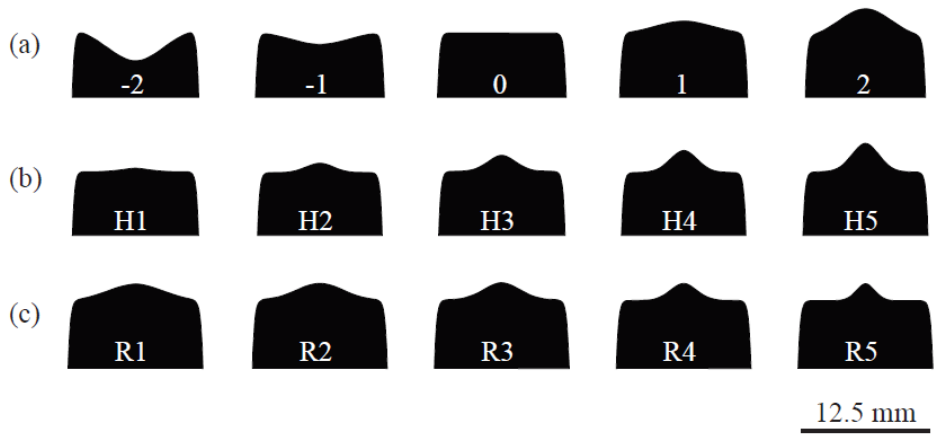

Figure 1.2 - Experimental model morphologies. (a) Convex-concave tooth model morphologies. (b) Tooth model morphologies with a cusp of varying height. (c) Tooth model morphologies with a cusp with a base of varying width.

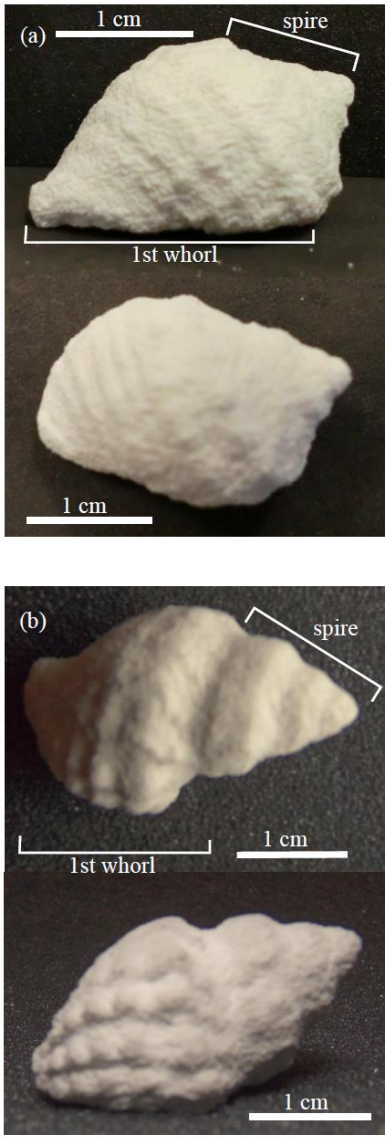

Figure 1.3 - Snail shell prototypes. (a) A printed copy of Nucella ostrina in dorsal and lateral view. (b) A printed copy of N lamellosa in a dorsal and lateral view.

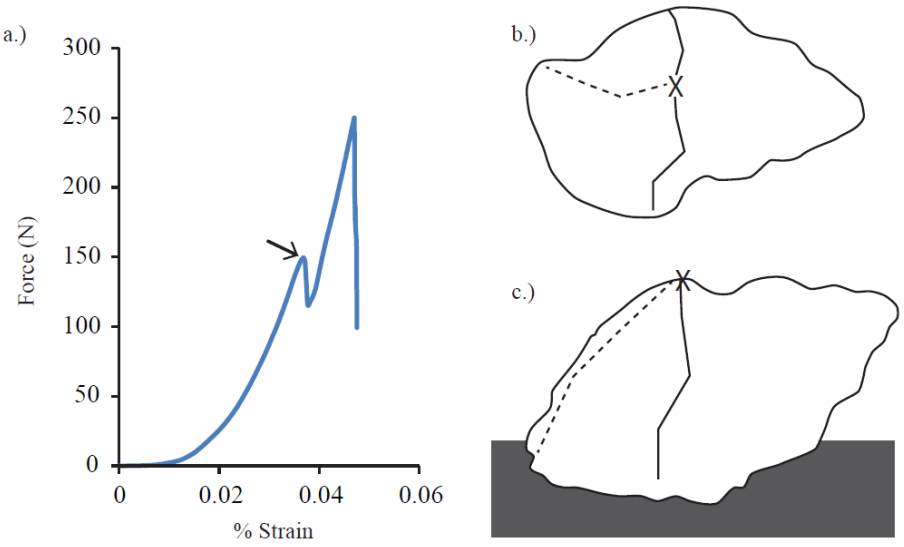

Figure 1.4 – Shell failure a) Example of load versus strain curve demonstrating brittle failure. Strain was calculated based on the displacement of the tooth model. Arrow indicates point at which initial load of failure was measured. b) Common locations of crack formation as seen in dorsal and (c) lateral view. Cracks most often formed radiating from the point of loading (indicated by an x) around the body whorl normal to the long axis of the shell (solid line). On some occasions, cracks would also radiate from the point of loading along the long axis of the shell towards the siphonal notch (broken line).

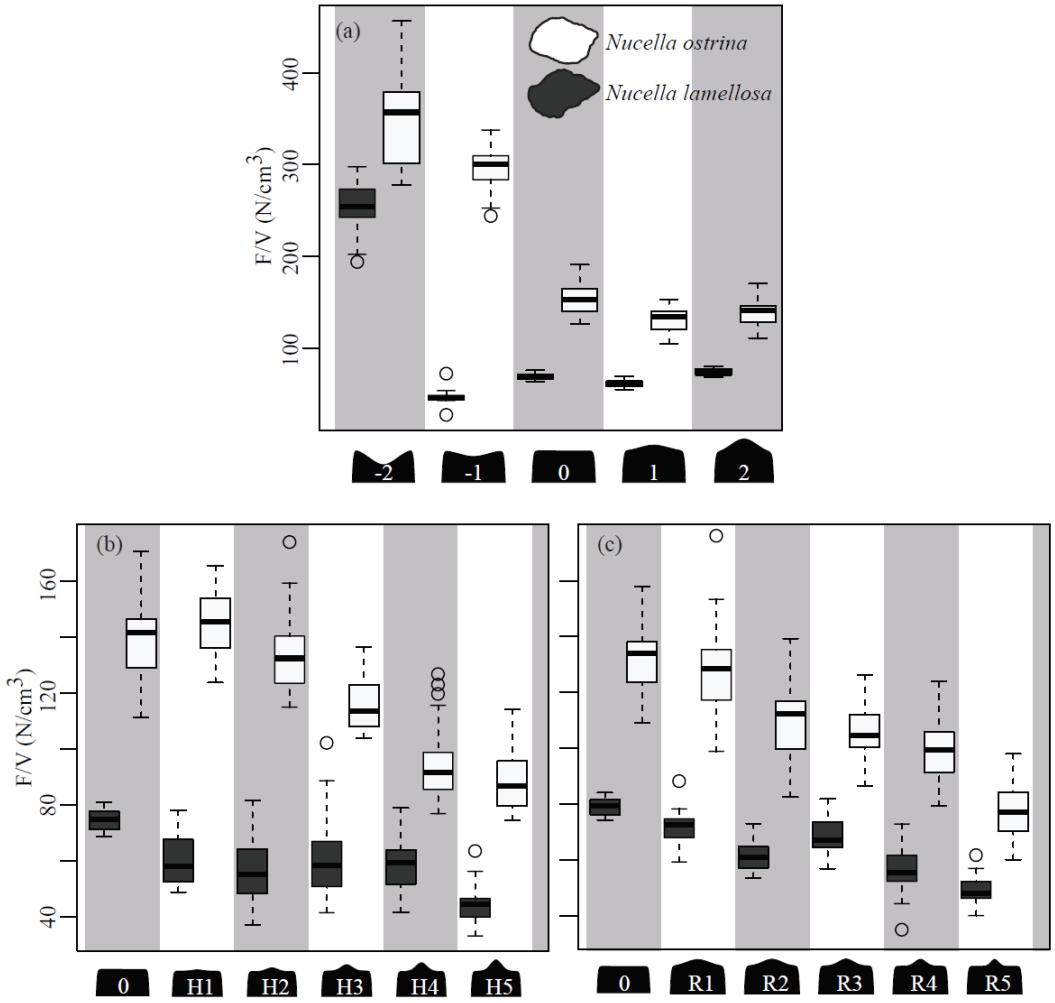

Figure 1.5 - Comparison of F/V (in N/cm3) needed to initiate crack propagation in (a) convex-concave tooth models, (b) tooth models with cusps of varying heights, and (c) tooth models with cusps with bases of varying widths. Boxplots demonstrate distribution of F/V for *Nucella ostrina* (white) and *N. lamellosa* (dark grey); heavy middle dash indicate medians, the upper and lower edge of the box bound the second and third quartiles (25%) of the data, respectively, the whiskers indicate maximum quartile ranges, and circles represent outlying data points.

Table 1.1 - Comparison of tooth model parameters and force of initial failure. Also reported are the radius of curvature of the occlusal surface of the tooth models, and force of initial failure scaled by both shell volume and by the cube root of volume, to estimate energy release.

shape	*h*	*r*	radius of curvature	species	F (N)	± SD	F/V (N/m^3)	± SD	$F/\sqrt[3]{V}$ (N/m)	± SD
-2	0.5	0.4	0.4	*N. ostrina*	379.5724	53.72428	351.4559	49.7447	369.9588	52.363583
				N. lamellosa	272.9533	28.76839	252.7346	26.6374	290.444	28.036758
-1	0.25	0.4	0.8	*N. ostrina*	319.3861	26.07399	295.7279	24.14258	311.2969	25.413603
				N. lamellosa	57.84152	7.616884	47.63296	7.789641	61.54796	8.1048107
0	0	0.4	0	*N. ostrina*	150.5768	14.28893	139.423	13.23049	146.7631	13.927032
				N. lamellosa	61.73644	3.061052	74.38125	3.688014	65.69246	3.2572019
1	-0.25	0.4	-0.8	*N. ostrina*	166.9758	18.94995	154.6072	17.54625	162.7467	18.469997
				N. lamellosa	57.6576	2.697822	69.46699	3.250388	61.35226	2.8706967
2	-0.5	0.4	-0.4	*N. ostrina*	142.7502	14.45487	132.1761	13.38414	139.1347	14.088765
				N. lamellosa	51.25308	3.394624	61.7507	4.089908	54.53734	3.6121485
H1	0.05	0.1	1	*N. ostrina*	157.4508	12.03038	145.7877	11.13924	153.4629	11.72568
				N. lamellosa	50.09194	7.678509	60.35174	9.251215	53.30179	8.170542
H2	0.15	0.1	0.333	*N. ostrina*	145.6952	15.94638	134.903	14.76517	142.0052	15.5425
				N. lamellosa	47.41974	9.072596	57.13222	10.93084	50.45836	9.653961
H3	0.25	0.1	0.2	*N. ostrina*	125.9957	11.13195	116.6627	10.30736	122.8045	10.85001
				N. lamellosa	50.75364	11.67119	61.14896	14.06168	54.00589	12.41908
H4	0.35	0.1	0.143	*N. ostrina*	103.0125	14.41341	95.38196	13.34575	100.4035	14.04836
				N. lamellosa	48.52072	7.276258	58.4587	8.766576	51.62989	7.742515
H5	0.45	0.1	0.111	*N. ostrina*	96.04356	11.74515	88.92922	10.87514	93.61102	11.44768
				N. lamellosa	36.6542	5.42367	44.16169	6.534542	39.00297	5.771215
R1	0.25	0.3	0.6	*N. ostrina*	145.9132	24.15595	135.1049	22.36662	142.2176	23.54414
				N. lamellosa	54.38548	5.915001	65.52467	7.126507	57.87046	6.29403
R2	0.25	0.2	0.4	*N. ostrina*	123.2947	17.48208	114.1617	16.18711	120.1719	17.0393
				N. lamellosa	44.44848	5.362634	53.55239	6.461005	47.2967	5.706268
R3	0.25	0.1	0.2	*N. ostrina*	116.0134	14.04102	107.4199	13.00095	113.0751	13.6854
				N. lamellosa	51.09252	6.843818	61.55725	8.245564	54.36649	7.282365
R4	0.25	0.05	0.1	*N. ostrina*	107.1584	16.07942	99.22076	14.88835	104.4444	15.67217
				N. lamellosa	38.93308	8.411486	46.90733	10.13432	41.42788	8.950487
R5	0.25	0.025	0.05	*N. ostrina*	78.03683	12.77552	72.25633	11.82919	76.06036	12.45195
				N. lamellosa	31.6202	4.771286	38.09663	5.748537	33.6464	5.077026

Chapter 2. FINITE ELEMENT MODELING OF OCCLUSAL VARIATION IN DUROPHAGOUS TOOTH SYSTEMS

Crofts, S.B. (2015) Finite element modelling of occlusal variation in durophagous tooth systems. *J Exp Biol* (DOI 10.1242/jeb.120097).

In addition to breaking hard prey items, the teeth of durophagous predators must also resist failure under high loads. To understand the effects of morphology on tooth resistance to failure, finite element models were used to examine differences in total strain energy (J), first principal strain, and the distribution of strains in a diversity of canonical durophagous tooth morphologies. By changing the way loads were applied to the models, I was also able to model the effects of large and small prey items. Tooth models with overall convex morphologies have higher in-model strains than those with flat or concave occlusal surface. When a cusp is added to the tooth model, taller or thinner cusps increase in-model strain. While there is little difference in the relationships between tooth morphology and strain measurements for most models, there is a marked difference between effects of the large and small prey loads on the concave and flat tooth morphologies. Comparing these data with measurements of force required by these same morphologies to break prey items illustrates functional tradeoffs between the need to prevent tooth failure under high loads by minimizing in-tooth strain versus the drive to reduce the total applied force.

Key words: durophagy, tooth morphology, finite element analysis (FEA)

2.1 INTRODUCTION

Teeth are intimately involved in food acquisition and processing, therefore preventing tooth fracture, and the resultant loss of tooth function, is important. Work on fracture failure during food processing has focused primarily on bunodont

teeth, such as the molars of humans or other primates. The dentistry community has been a strong motivator for this, with a focus on better understanding the mode of fracture in bunodont teeth under various loads. For example, radial cracks are the most prevalent mode of failure in simple bi-layered spheres when loaded with hard food items, but marginal cracks and semilunar chipping dominate when loading with softer foods (Qasim et al. 2005; Qasim et al. 2007). Other work has focused on the role diet has played in human evolution. Primates that have to process large hard prey-items prevent tooth fracture by thickening the enamel caps of their teeth (Lucas et al., 2008). In fact, enamel thickness is one of the aspects of tooth morphology that determines the mode of tooth failure in generalized bunodont teeth (Lawn and Lee, 2009). In addition to resisting tooth failure, hominid tooth morphology was also influenced by the ability to break food items (Berthaume et al., 2011). A mix of different cusp morphologies on the same tooth, as opposed to all sharp or all blunt for instance, takes these opposing evolutionary pressures into account to optimize bunodont tooth function: creating high stress in prey objects while minimizing stresses in the tooth enamel (Berthaume et al., 2013; Berthaume et al., 2014).

While the bulk of tooth fracture literature focuses on bunodont dentitions, the function of other tooth morphologies has also been addressed, for example carnivores, especially hypercarnivores, have modified teeth to pierce and cut soft tissues. Work on piercing teeth has focused on the length and bladed aspects of puncturing tooth morphology, approaching tooth failure as a functional trade-off with puncturing ability (Freeman and Lemen, 2007; Van Valkenburg and Ruff, 1987). At the same time, other work has looked at more detailed aspects of morphology, such as tooth composition, and found that the smoothed tips of conical puncturing teeth reduces the likelihood of chipped teeth, which allows for thinner enamel (Lawn et al., 2013). However, when puncturing soft tissues, stress concentrations are shifted to the margins of tooth crowns. These stress concentrations can lead to failure, but may be mitigated by the addition of a cingulum, a reinforced ledge of enamel that wraps around the base of many

mammalian teeth (Anderson et al., 2011). Cutting teeth, like shark teeth or the carnivore carnassials, are often notched. These notches reduce the work needed to process malleable prey (Anderson and LaBarbera, 2008; Anderson, 2009; Anderson and Rayfield, 2012) though they can also concentrate stresses in the tooth, thus making tooth failure more likely (Whitenack et al., 2011).

Bunodont dentition shears and pulps food, caniniform teeth and carnassials pierce and cut through flesh, but crushing teeth have the straightforward job of transmitting the compressive force required to shatter a prey item. Across vertebrate taxa, crushing teeth are characterized with subjective, and ultimately uninformative, stereotypical terms, "flattened", or "molariform" (Mara et al., 2009; Mehta, 2009; Summers, 2000; Wilga and Motta, 2000), that serve to obscure the great diversity of tooth forms associated with durophagous diets. Teeth associated with hard-prey crushing diets can vary in occlusal convexity, and some even have cusps (Fig. 2.1). However, this diversity of tooth forms is not entirely expected - some tooth shapes are better able to crush hard prey than others, which should lead to convergence on this design (Crofts and Summers, 2014). Of course, the ability of teeth to crush prey items is only one selective pressure affecting tooth shape; the ability to withstand high forces without breaking must also be shaping teeth. The arms-race between durophagous predators and their prey has had a profound impact on ecological structures throughout time (Vermeij, 1977), but the question still stands: what evolutionary pressures have shaped hard-prey crushing teeth through time?

The goals of this paper are threefold: to determine the effect of occlusal concavity/convexity on strain in a crushing tooth, to quantify the role of a centrally located stress concentrator on strain in the tooth, and to determine whether the ability of different tooth shapes to resist strain is sensitive to variations in prey size. To do this, I have analyzed three series of canonical tooth shapes as Finite Element (FE) models, with each series varying by a single aspect of tooth morphology (Fig. 2.2). In this way I can determine how changes in tooth

morphology will affect strain distribution in teeth subjected to occlusal loads simulating either small or large hard prey items.

2.2 METHODS AND MATERIALS

I used Finite Element Analysis (FEA) to study a range of canonical tooth models that mimic durophagous tooth morphologies. I generated three series of models by rotating a line (eq 1.1) around the y-axis (Fig. 2.3) and changing the parameters of the equation.

$$y = -(x^{32} - h \times exp^{-(\frac{x^2}{r})}) \tag{1.1}$$

For the first series, I varied the overall occlusal morphology from a deep concave surface, to one that was flat, to a highly convex occlusal surface. This was achieved by setting r =0.4, so that the added curve would cover the whole face of the model's occlusal surface, and varying h from -0.5 to 0.5 in increments of 0.1. This resulted in 11 morphologies (Fig. 2.2A): 5 of varying concavity, one flat occlusal surface, and 5 with various degrees of convexity. In the second series, I added cusps of varying heights to the center of the occlusal surface of the flat tooth morphology. The width of the base of the cusp was constrained by setting r = .01, and h ranged from 0 (no cusp) to 0.5, increasing in increments of 0.05. This generated another 11 shapes (Fig. 2.2B) with cusps of increasing height. The final series of models also had central cusps, but varied in the width of the base of the cusp. Cusp height was fixed (h = 0.25), and the base of the cusp ran from r = 0.4, which covers most of the occlusal surface, to the narrowest cusp where r = 0.01. Beginning at r = 0.4, the value of r decreased by 0.05 between each progressive model morphology until r = 0.01. From that point, r decreased by 0.02 until r = 0.02, which was halved (r = 0.01) to create the narrowest cusp. This resulted in a series of 12 models (Fig. 2.2C).

Tooth models were constructed in the axisymmetric work-flow in COMSOL Multiphysics (ver. 4.3). To better reflect the structure of real teeth, models were constructed to have an outer layer of brittle, enameloid-like material, over a body of more ductile, dentine-like, material. This was accomplished by duplicating and scaling the initial equation (Fig. 2.3) in the course of model construction. I did not include a pulp cavity in the tooth models, following Anderson et al.'s (2011) reasoning that dentine is soft enough to allow for all enameloid deformation. There is little data in the literature on the material properties of non-mammalian tooth tissues, so I used averaged values taken from Whitenack et al. (2010). I set the Young's Modulus of the enameloid layer to 70.745 GPa and the Young's Modulus of the dentine body to 25.465 GPa, and used 0.3, an accepted estimate for most biological materials, as the Poissons's ratio for both materials. I used COMSOL's built-in mesh feature to mesh the models, and set the mesh fineness such that there were multiple elements across the depth of the enamloid layer (Fig. 2.3). To mimic tooth attachment, I anchored the base of the model (Fig. 2.3), allowing no translation or rotation.

Each model was subjected to two loading regimes (Table 2.1), both centered over the middle of the tooth model's occlusal surface and running perpendicular to the base of the tooth (Fig. 2.4). The first loading regime was designed to mimic prey items smaller than the tooth, or with a much smaller radius of curvature. This was achieved by defining the area of the occlusal surface being loaded as a circle with a set radius (0.05; Fig. 2.4A). For models with narrow cusps, this method of loading is unrealistic, since the load spreads down the sides of the cusp (Fig. 2.4B). To correct for this, loads were constrained to the tip of the cusp down to a fixed height, approximately the same depth as the small load reached in the convex models (~ -0.012345). The second loading regime mimics a prey item larger than the tooth or with a much larger radius of curvature. For this loading regime, loads were applied to the leading edge of the model to this same fixed height. For most models, those that were convex or possessing a cusp, this led only to a small change in the area being loaded, but not location of the load. For concave models, however, the large

prey item loading regime loads only the peripheral edges of the occlusal surface, versus the middle of the occlusal surface. Similarly, while the small prey item loading regime only loads the middle of the occlusal surface for the flat model, the large prey item loading regime spreads the load over the entire occlusal surface.

The brittle failure of teeth directed both the loading of the models as well as the types of measurements we could take. Since teeth fail as brittle solids, loads were scaled to the volume of the specific model for each test (Dumont et al., 2009) to allow for comparison between morphologies. Because total load depends only on the volume of the model being tested, not the area loaded, total loads were the same for both loading regimes for each individual model.

Similarly, we used only 1st principal strain, not Von Mises stresses, as that is more appropriate for brittle solids (Dumont et al., 2009). Maximum principal strain describes the magnitude of strain at the most deformed node in the model, and while there are three principal strains, I measured only the 1st principal strain because it was consistently the largest tensile strain, and therefore most likely to be associated with failure. It should be noted that because maximum principal strains deal with only a single node, there is the potential for these data to be misleading if the node is anomalous. In addition to the maximum 1st principal strain, I also gathered data on the total strain energy in each model. This is a measurement of the amount of energy that goes into the deformation of each shape. Since there is a threshold for any given material, past which it will break, teeth made of the same material should all have the same threshold. This means that teeth with a higher measured total strain energy will be more likely to pass that threshold and, thus, more likely to break. In the course of modeling, we generated heat maps demonstrating the distribution of strain in each model, allowing us to predict the most likely location of failure in each tooth model morphology.

2.3 RESULTS

For the concave-convex series of models under the small prey item loading regime, total strain energy increases as occlusal surfaces shift from concave to convex (Fig. 2.5A; Table 2.1). Maximum 1st principal strain follows a similar pattern, with concave shapes having low maximum 1st principal strain and convex shapes having high maximum 1st principal strain. Figure 2.6A shows the changes in 1st principal strain distribution for the convex-concave model series under the small prey item loading. While the magnitude of strain changes between model morphologies, there is little change in overall strain distribution. For all models in this series, strain is primarily concentrated in the enameloid around the area being loaded, and dissipates through both the enameloid layer and the dentine body.

There is a marked difference between the patterns of total strain energy and maximum 1st principal strain in the concave morphologies when comparing the large prey item loading regime to the small prey item loading regime. Under the large prey item loading regime, as models go from concave to flat there is a very slight increase in total strain energy and maximum 1st principal strain; the difference between the most concave model and the flat model is much less than that observed under the small prey item load (Fig 2.5B; Table 1). However, as expected given the similarity in loading areas, the overall pattern of increase in in total strain energy and maximum 1st principal strain for the convex morphologies under the large prey item loading regime is similar to the increases seen under the small prey item load regime in these same shapes (Fig. 2.5A; Table 1). Figure 2.7A shows the strain distributions for the convex-concave models under the large prey item load regime. For convex shapes, strain remains concentrated around the area being loaded, as in the small prey item load regime. As under the small prey item load regime, strain is distributed in both the dentine and enameloid of these models. For the concave models high strain is also concentrated under the site of applied load. However, in these shapes load is applied to the raised peripheral edges of the occlusal surface, and strain is more concentrated in the dentine than

the overlying enameloid layer. Additionally, rings of high strain develop around the base of both concave and flat models.

When models with central stress concentrators were loaded under the small prey item load regime, total strain energy increased as the cusp height increased. In contrast, the maximum 1st principal strain decreased as the stress concentrator height increased (Fig. 2.5C; Table 2.1). In the models themselves, 1st principal strain is concentrated in the dentine around the area under load and is distributed through both the enameloid and dentine in the immediate area. This pattern remains constant for all stress concentrator heights (Fig. 2.6B). For the large prey item loading regime, both total strain energy and maximum 1st principal strain increase with the height of the stress concentrator (Fig. 2.5D; Table 2.1). Because the area being loaded changes slightly, the distribution of 1st principal strain also varies slightly, but is always concentrated around the area being loaded (Fig. 2.6B). Strain is distributed through both the dentine and enameloid, but for morphologies with lower cusps there is more strain in the dentine layer, but the magnitude remains lower than the strain in the enameloid layer.

For the models with stress concentrators with bases that vary from wide to narrow, there is a similar pattern for both the large and small prey item loads (Fig. 2.5 E, F; Table 2.1). For both loads, there is little change in the magnitude of total strain energy or maximum 1st principal stain for most models. But there is a rapid increase in both metrics for the last three morphologies, those with the narrowest stress concentrators. For both loading regimes, 1st principal strain is concentrated around the area loaded, though this area varies slightly under the large prey item load regime (Figs 2.6C, 2.7C). For most tooth models, strain is distributed between the dentine and enamel layers, similar to the pattern seen in the other tooth model series. For the three morphologies with the narrowest stress concentrators, strain begins to form rings around the stress concentrator and is concentrated in the enameloid layer of the model under both loading regimes.

2.4 DISCUSSION

These results demonstrate the evolutionary pressure on hard prey crushing teeth to resist failure, but this is not the only factor influencing tooth morphology. Comparing these results to previous work on the crushing ability of teeth, there appears to be a trade-off in performance. Testing the force required to break brittle, morphologically identical, 3D printed shells by physical models of the same three series of canonical tooth models tested here, tells a different story of tooth optimization (Crofts and Summers, 2014). For large and small prey items, greater strains in convex teeth means a greater likelihood of crack formation than flat or concave teeth, but convex teeth required less force to break a prey items than flat or concave ones (Fig. 2.5A, B). Similar relationships are seen in the cusped tooth models: taller cusped teeth are better able to break prey but have higher strain values (Fig. 2.5C, D), and the thinnest cusps show much higher strain values but are more effective at inducing prey failure (Fig. 2.5E, F). Given the trade-offs between tooth morphologies that can effectively fracture prey items and morphologies that will resist tooth failure, we might expect that intermediate, "ideal" tooth morphologies would be the de facto tooth shape for hard-prey consumers. This, however, is not the case as there is a wide range of durophagous tooth morphologies.

One explanation for this variation in tooth morphology is the effect of prey shape, size, and material properties on tooth failure. Smaller prey generate loads that show a more pronounced change in both maximum strain energy and 1st principal strain as tooth models go from concave to flat, than larger prey items. Finite element models of 4-cusped bunodont teeth loaded by brittle spheres of varying sizes showed a similar pattern of size mediated variation in strain (Berthaume et al., 2014). Similarly, hemispherical tooth models worn flat were able to achieve a higher load to critical failure when loaded by flat surfaces than by rounded surfaces (Keown et al., 2012). The interaction between the flat indenter and the increasingly flat occlusal surface serves to spread the applied load (Ford et

al., 2009). Given that the concave tooth morphologies of the present study behave similarly to the flat tooth morphology under the large prey loading regime, spreading the applied load will also increase the load to critical tooth failure. In this way, the gradation of concave to flat tooth morphologies represents a greater range of tooth morphospace open to animals that consume large prey items than may be available to those who consume relatively smaller prey items. Since concave tooth morphologies also spread the applied load, they can reduce the impact of tooth wear, and allow for increased tooth usage when processing larger prey items as well. While flatter surfaces spread loads and increase the load to critical failure, enamel that has been worn thin can flex and lead to subsurface cracks when loaded by a rounded indenter. Additionally, the discontinuity caused by the flat, worn surface can be prone to chipping, even with a flat indenter (Ford et al., 2009).

It should be noted that this is a discussion of the effects of loading and morphology on a single tooth. Loads can also be distributed across multiple teeth, reducing the applied force to any one tooth. Multiple teeth abutting each other can also allow for stresses and strains to be distributed from one tooth to another, redirect forces to teeth or portions of teeth less likely to fail, and improve overall tooth stability (Nobiling, 1977; Ramsay & Wilga, 2007). The present study is a first step in understanding the effects of loading on hard-prey crushing teeth, and further work is needed to understand how the interaction of multiple teeth would affect the patterns of strain distribution and magnitude.

The patterns of strain that we predict from the finite element models is reflective of real world failure regimes in physical models and in real teeth. When crushing large prey the highest strain was concentrated in rings around the body of the tooth, for flat and concave teeth. A similar ring of concentrated strain can be seen around the base of the narrowest cusps for large and small prey, unlike other cusp morphologies where high strains are concentrated at the tip of the cusp. This pattern of strain distribution is similar to stress distributions seen in bi-layered epoxy models, which were shown to develop into ring cracks (Qasim et al., 2005). Additionally, a shift in strain to the margins of the model, as seen here in the

concave and flat tooth morphologies, can lead to failure at the edge of the model (Qasim et al., 2007). This susceptibility to ring cracks and edge failure may be a reason that concave tooth morphologies are not as common as convex morphologies in nature. Finally, in cusped teeth, this strain pattern indicates a discontinuity between the body of these tooth models and the cusp and is a site of likely failure.

Having teeth that resist failure is less important for animals that replace teeth frequently than for those who only rarely replace teeth, so the frequency of tooth replacement should be tied to tooth morphology. However, in durophagous animals it is also important to maintain functional tooth sites, which should reduce the rate of tooth replacement (Dalrymple, 1979). This strategy of reducing the rate of tooth replacement to prolong individual tooth function should constrain tooth morphology, favoring tooth morphologies that will be less likely to break. Some animals have developed an interesting solution to the competing pressures to replace teeth infrequently, maintaining function, and to increase the rate of tooth replacement, to remove damaged teeth, by developing a pattern of tooth replacement that maintains one functional crushing surface at a time while replacing another (Neenan et al., 2014). In these lineages, this may allow for more flexibility in replacement rate and morphology.

The results of finite element modeling are only as good as the data put into the model. Our model relies on stiffness values for teeth from two species of shark that are not durophagous (Whitenack et al., 2010). There is evidence for a difference in the hardness of tooth materials for cutting versus tearing shark teeth (Enax et al., 2012), and fiber orientation in the enamel of crushing teeth does differ from other tooth types, which may allow these crushing teeth to be more resistant to compression (Preuschoft et al., 1974). Changing the material properties of the different layers of the tooth models could affect how strain is transmitted from one layer to the other and change the magnitude and patterns of maximum principal strain distribution in the models. We also only tested a single thickness of enamel across all tooth models. In mammalian bunodont teeth variation in enamel thickness plays an important role in preventing tooth failure due to wear versus

brittle fracture (Lawn and Lee, 2009). Neither the effects of changing both tooth material properties nor of varying enamel thickness are addressed in this study and should be pursued in future work. The present study serves as a step towards understanding how shape affects strain distribution through hard-prey crushing teeth, and how this may influence the evolution of different specialized tooth morphologies.

2.5 TABLES AND FIGURES

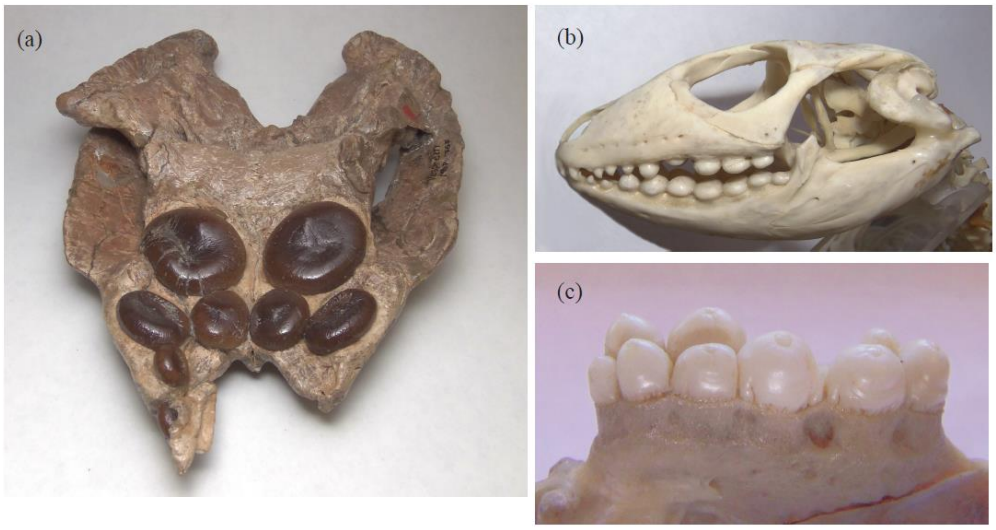

Figure 2.1 - Diversity of durophagous tooth morphologies. Examples of tooth morphology from a diverse range of vertebrate taxa demonstrating A) concave teeth in the extinct sauropterygian, *Placochelys placodonta* †, B) convex teeth in a molluscivorous lizard (*Dracaena sp.*), and C) cusped teeth in the wolf eel (*Anarrhichthys ocellatus*).

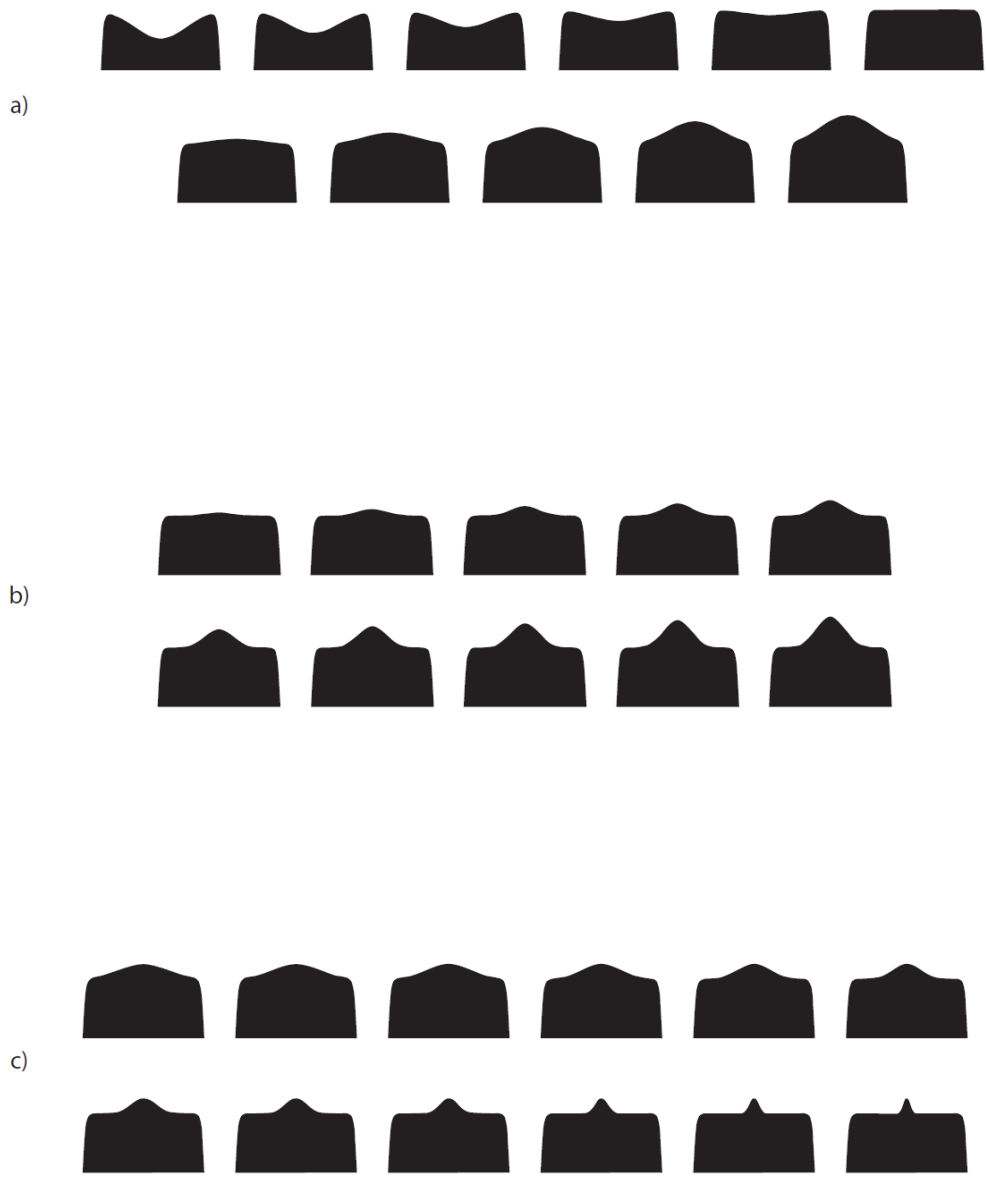

Figure 2.2 - Three series of tooth model morphologies. A) Concave-convex series of tooth models. B) Series of tooth models with cusps of varying height at center of occlusal surface. C) Series of tooth models with cusps of varying width at center of occlusal surface.

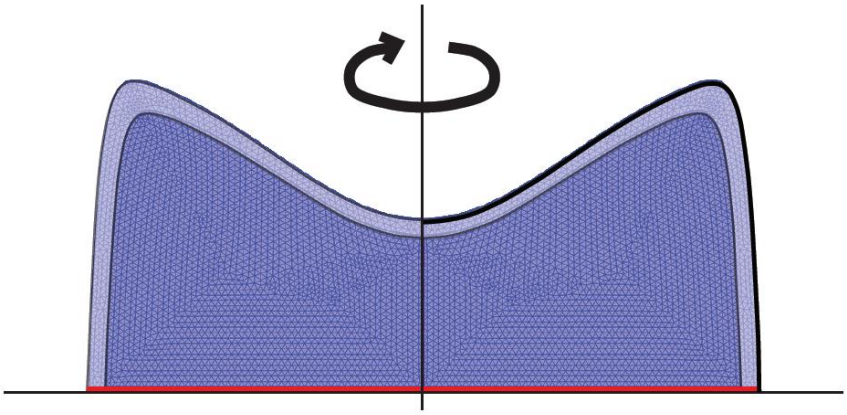

Figure 2.3 - Finite element model construction. The outer layer of the tooth model was defined by eq 2.1 (bold line) and delineation between the outer layer (light blue) and the inner core (dark blue) was generated by duplicating and scaling the initial equation. The outer layer was assigned material properties to mimic an enameloid-like material and the inner core was modeled as a dentine-like material. For all models, the base of the tooth was anchored (red line) and everything was rotated about the y-axis (arrow) to create 3D models.

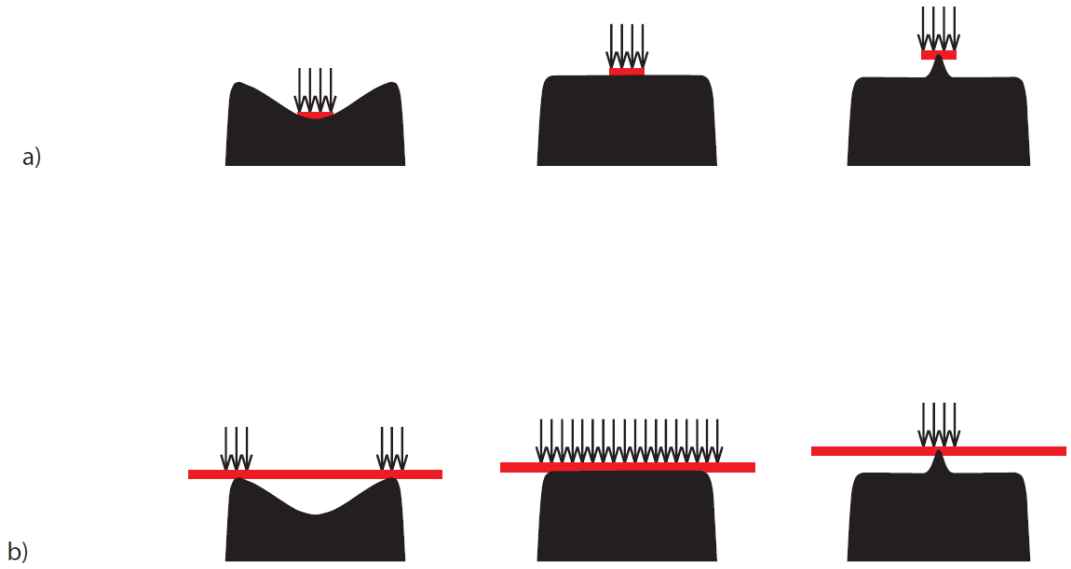

Figure 2.4 - Examples of small and large prey item loading regimes. Red bars and arrows represent location and direction of applied load for the A) small and B) large loading regimes across a representative range of tooth model morphologies.

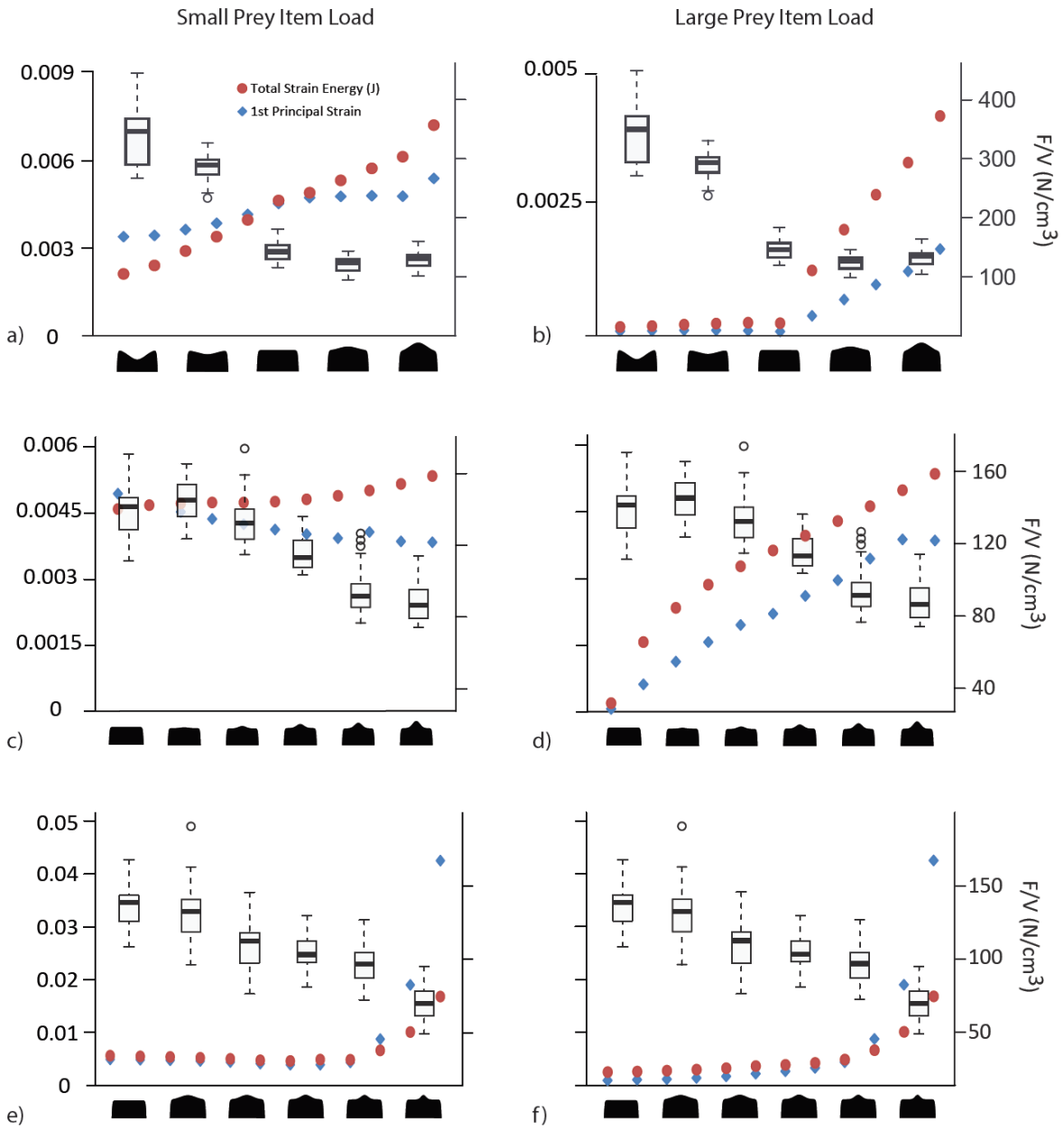

Figure 2.5 - Total strain energy (J) and maximum 1st principal strain for all tooth models under small and large prey item loading regimes compared to load required to break a sample prey item. For each graph, tooth morphologies are shown along the x axis. Values on the left hand y-axis correspond to both total strain energy (J; in red) and 1st principal strain (unitless; in blue). Values on the right-hand y-axis correspond to box-whisker plots (dark bar represents medians, box spans second and third quartiles, whiskers represent quartile bounds, and open circles represent outlying data) showing the

force (F; in Newtons (N)) normalized by shell volume (V; in cm^3) needed to induce failure in a snail shell as a sample prey item (see Crofts and Summers, 2014). Data for the concave-convex series of tooth models under a small loading regime (A) and under a large loading regime (B). Data for the series of tooth models with a cusp of varied height under a small loading regime (C) and a large loading regime (D). Data for the series of tooth models with wide-narrow cusps under a small loading regime (E) and under a large loading regime (F).

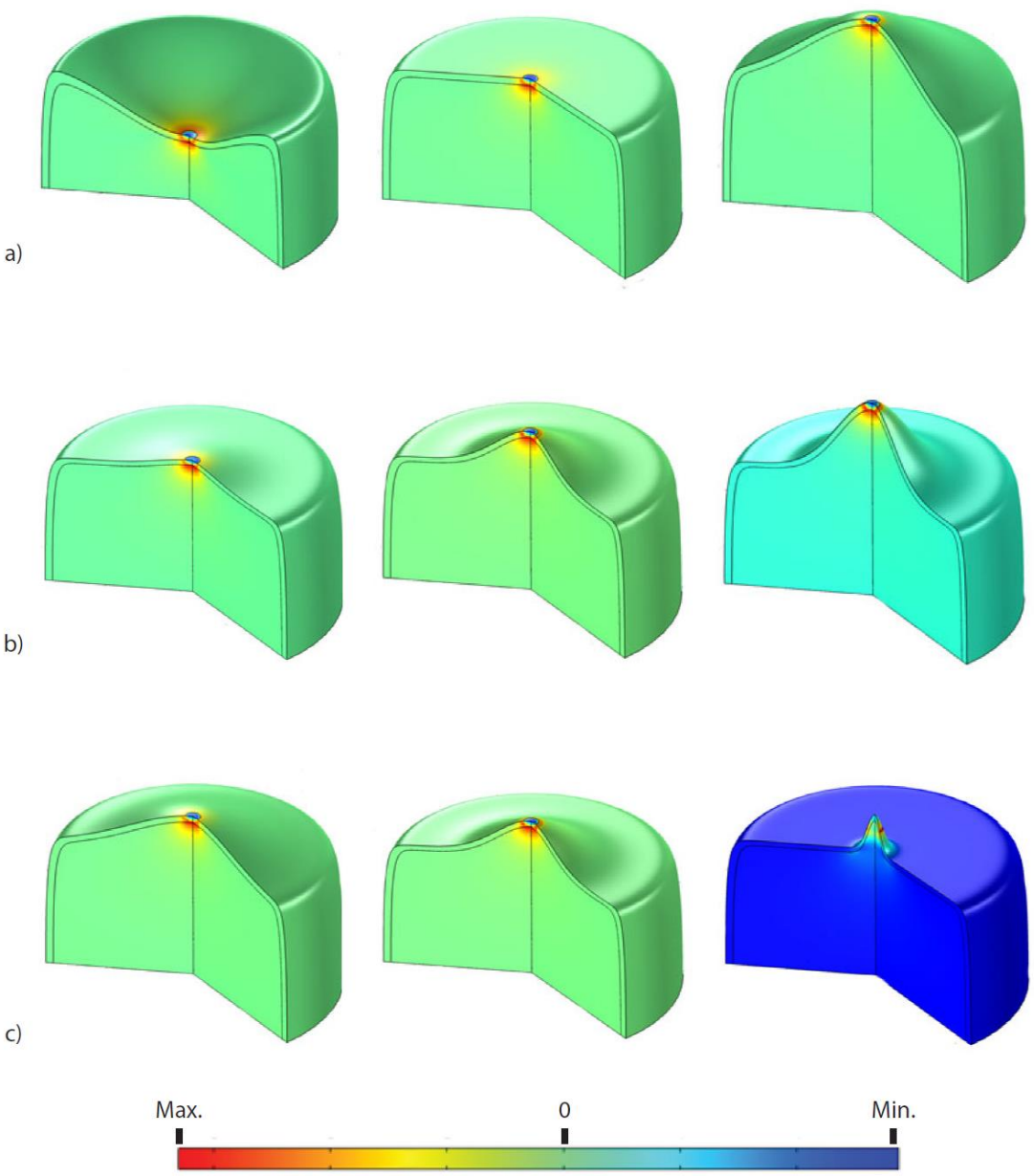

Figure 2.6 - Distribution of 1st principal strain in tooth models with load representing a small prey item. A) Representative morphologies from the concave-convex series of tooth models. B) Representative morphologies from the series with a cusp of variable height. C) Representative morphologies from the series with a cusp with a variable base width.

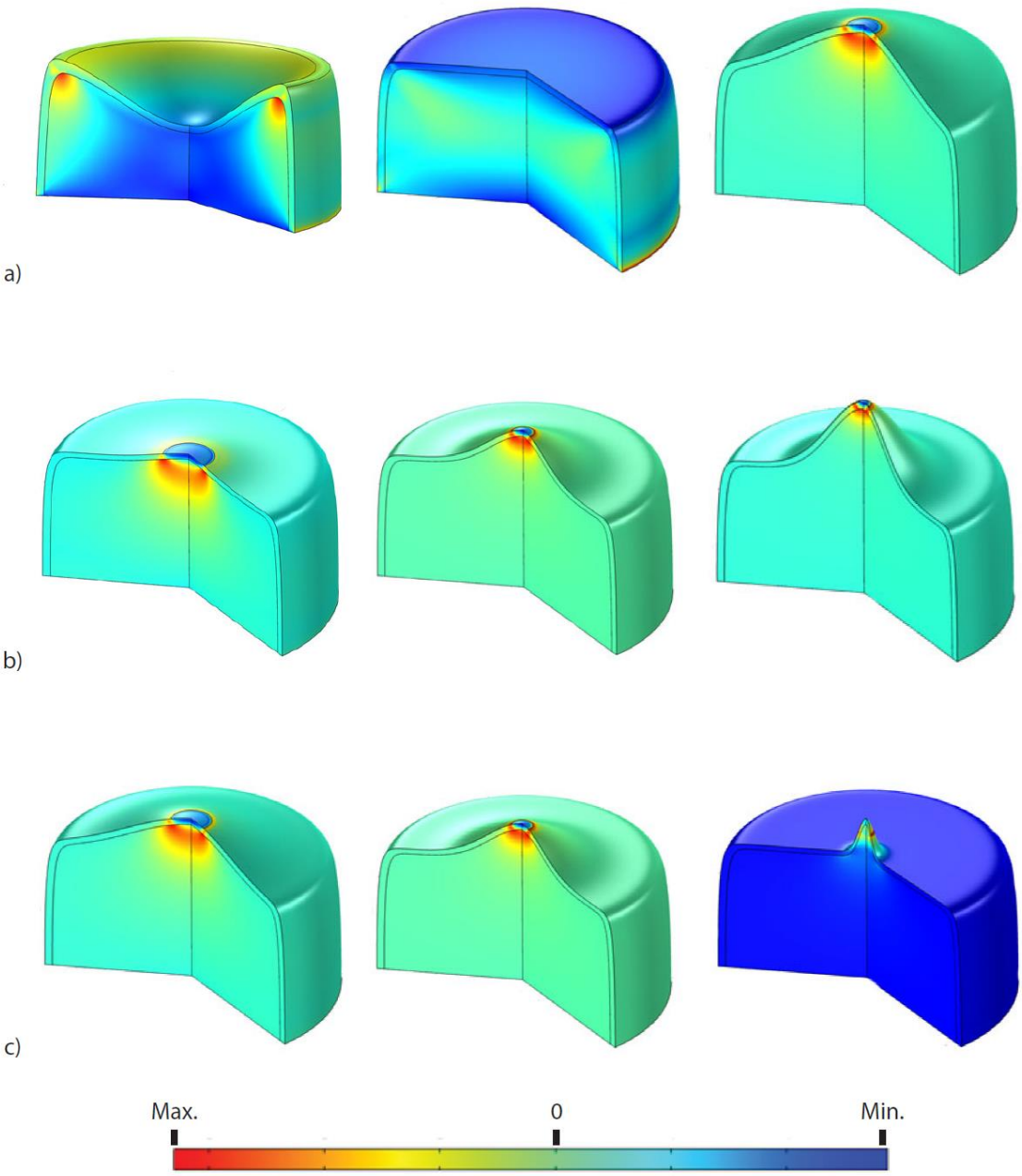

Figure 2.7 - Distribution of 1st principal strain in tooth models with load representing a large prey item. A) Representative morphologies from the concave-convex series of tooth models. B) Representative morphologies form the series with a cusp of variable height. C) Representative morphologies from the series with a cusp with a variable base width.

Table 2.1 - Parameters (h and r), applied load, maximum 1st principal strain, and total strain energy (J) for each model.

Tooth series and number	*h*	*r*	Applied load (N)	Maximum 1st principal strain	Total train Energy(J)
Concave-convex 1	-0.5	.4	437.67	3.37E-03	2.10E-03
Concave-convex 2	-0.4	.4	465.718	3.41E-03	2.39E-03
Concave-convex 3	-0.3	.4	506.317	3.61E-03	2.88E-03
Concave-convex 4	-0.2	.4	540.635	3.83E-03	3.37E-03
Concave-convex 5	-0.1	.4	574.955	4.12E-03	3.94E-03
Concave-convex 6	0	.4	609.279	4.50E-03	4.60E-03
Concave-convex 7	0.1	.4	612.222	4.69E-03	4.86E-03
Concave-convex 8	0.2	.4	646.533	4.74E-03	5.28E-03
Concave-convex 9	0.3	.4	680.846	4.76E-03	5.69E-03
Concave-convex 10	0.4	.4	715.165	4.74E-03	6.09E-03
Concave-convex 11	0.5	.4	749.49	5.35E-03	7.16E-03
Height 1	.1	0	577.912	4.94E-03	4.59E-03
Height 2	.1	0.05	586.718	4.68E-03	4.68E-03
Height 3	.1	0.1	595.522	4.53E-03	4.72E-03
Height 4	.1	0.15	604.326	4.37E-03	4.74E-03
Height 5	.1	0.2	613.13	4.25E-03	4.74E-03
Height 6	.1	0.25	621.934	4.13E-03	4.76E-03
Height 7	.1	0.3	630.738	4.02E-03	4.81E-03
Height 8	.1	0.35	639.54	3.93E-03	4.89E-03
Height 9	.1	0.4	648.349	4.07E-03	5.01E-03
Height 10	.1	0.45	657.152	3.86E-03	5.16E-03
Height 11	.1	0.5	665.955	3.84E-03	5.34E-03
Width 1	0.35	0.25	658.861	4.94E-03	5.63E-03
Width 2	0.3	0.25	653.395	4.86E-03	5.51E-03
Width 3	0.25	0.25	647.18	4.75E-03	5.38E-03
Width 4	0.2	0.25	640.068	4.62E-03	5.22E-03

Width 5	0.15	0.25	631.812	4.43E-03	5.02E-03
Width 6	0.1	0.25	621.934	4.13E-03	4.76E-03
Width 7	0.08	0.25	617.287	3.94E-03	4.64E-03
Width 8	0.06	0.25	612.012	3.93E-03	4.89E-03
Width 9	0.04	0.25	605.754	4.37E-03	4.86E-03
Width 10	0.02	0.25	597.599	8.77E-03	6.64E-03
Width 11	0.01	0.25	591.834	1.90E-02	1.01E-02
Width 12	0.005	0.25	587.756	4.25E-02	1.68E-02

Chapter 3. CHANGES IN TOOTH OCCLUSAL MORPHOLOGY IN THE DUROPHAGOUS MARINE REPTILES, THE PLACODONTIDAE (REPTILIA, SAUROPTERYGIA)

Key words: Placodont, tooth morphology, durophagy

3.1 INTRODUCTION

3.1.1 *Introduction*

Placodonts are a group of extinct marine reptiles that lived from the lower to late Triassic (Olenekian-Rhaetian), which originated in shallow coastal waters of the Western Tethys, and expanded east (Fig. 3.1; Neenan et al., 2013). Dental morphology is one of the key characters for identifying Placodontia, though initial descriptions of the teeth identified them as fish rather than reptiles (Owen, 1858). The link between tooth morphology and diet, enlarged flattened teeth for crushing and grinding, narrow pointed teeth for puncturing, and bladed teeth for cutting flesh, has been qualitatively demonstrated in extant taxa and used to infer diet in a range of extinct taxa (Anderson, 2009; Anderson and LaBarbera, 2008; Crofts & Summers, 2014; Kelley & Motani, 2015; Massare, 1987). Based on tooth morphology, placodonts have always been inferred to be durophagous predators, consuming hard prey by crushing their shells. This proposed durophagous lifestyle is further supported by the prevalence of hard-shelled prey items found in the same depositional environments as placodont remains (Assmann, 1937; Blake & Hagdorn, 2003), though there is some dispute (Diedrich, 2011). Durophagy, however, is a very specialized diet and is associated with a suite of other adaptations, such as the placement of the

teeth, deep or robust skull architecture, and expanded temporal areas for muscle attachment (Dalrymple, 1979; Rieppel, 2002), as well as modified tooth morphology.

Given the relationship between diet and tooth morphology, and specialization for durophagy within the placodont lineage, it is not surprising that we see overall changes in tooth size and occlusal shape (Owen, 1858; Rieppel, 1995) and in tooth position (Mazin, 1989) across the phylogeny. However, apart from qualitative observations that teeth are "low," "spherical," or "blunted" in groups closer to the root of the tree and "subspherical," "hemispherical," "with rounded edges," "flat," or "flatter" in more nested groups (Mazin, 1989; Neenan, et al., 2013; Neenan, et al., 2014; Neenan, et al., 2015; Nosotti & Pinna, 1999; Owen, 1858; Rieppel, 2000; Rieppel, 1995), little has been said about changes in the occlusal morphology of teeth within the placodont lineage.

Variation in occlusal morphology, which can be quantified by fitting a circle or sphere to the occlusal surface and measuring the radius of curvature (RoC), can have a measurable effect on tooth function. Flat teeth (with an infinitely large RoC) will be able to break shelled prey items with less force than concave or cupped (negative RoC) tooth morphologies, and with as much or less force than convex or cusped teeth (positive RoC; Crofts & Summers, 2014). However, greater occlusal convexity or more pointed crowns or cusps (small, positive RoC) will make tooth failure more likely under high loads compared to flat or concave surfaces, which are better able to diffuse in-tooth strain and can localize damage (Crofts, 2015; Lee et al., 2011; Qasim et al., 2004).

Based on these observed trade-offs, it is possible to predict an 'optimal' shape for durophagous teeth: a tooth with a flat or shallowly convex occlusal surface (large, positive RoC) which can both effectively crush shelled prey items while also resisting tooth failure. Given the

dietary specialization in the placodontiform lineage, measured occlusal morphologies should approach this 'optimum' as taxa become more specialized for durophagy. Occlusal morphologies that vary from the predicted tooth morphology may suggest a different, further specialized, diet or indicate that some other aspect of dental morphology or natural history is at play. The goals of this paper are threefold: 1) to quantify the occlusal morphology of placodont teeth, 2) to compare quantitative patterns of change to previously observed qualitative patterns of change, and 3) to determine if more nested groups of placodonts converge on the 'optimal' tooth morphology as predicted by the functional models.

3.1.2 *Background*

The placodontiformes (Fig. 3.2) consists of the placodonts and their sister taxon, *Palatodonta bleekeri*, which does not have crushing teeth. Instead, the teeth of this species have a more plesiomorphic condition: teeth are tall, narrow, and pointed. Tying *P. bleekeri* to the placodonts is the presence of a single row of similarly shaped teeth on the palatine bone (Neenan et al., 2013). This indicates that in the earliest common ancestor Placodontiformes was probably not specialized to eat hard prey, but more likely ate soft-bodied invertebrate prey items (Massare, 1987).

The Placodontia are typically divided into two groups: the unarmored Placodontoidea and the armored Cyamodontoidea. The placodontoids are a paraphyletic group consisting of two genera: *Paraplacodus*, at the root of the placodont tree, and *Placodus*, as a sister taxon to the Cyamodontoidea (Fig. 3.2; Rieppel, 2000). Both *Paraplacodus* and *Placodus* have a set of procumbent premaxillary teeth, thought to be for grasping prey living on-top of the substrate, separated by a diastema from the crushing teeth of the maxilla and palatine. While tooth arrangement is similar in these two groups, *Paraplacodus* has been typically considered to have

an overall more plesiomorphic tooth morphology (Mazin, 1989; Rieppel, 1995). The battery of crushing teeth in the upper of jaw of *Paraplacodus* consists of seven pairs of maxillary teeth, described as being low or round, each with a persisting central, conical cusp, and four pairs of palatine teeth, described as slightly larger than the maxillary teeth with an overall low, subspherical profile and similar conical cusps or blunt crowns (Fig. 3.3a; Mazin, 1989; Rieppel, 2000).

Compared to *Paraplacodus*, *Placodus* has reduced the number of crushing teeth, most often with four pairs of maxillary teeth, and three pairs of palatine teeth, though tooth counts vary slightly by specimen and species (Fig. 3.3b; Mazin, 1989; Rieppel, 1995). Descriptions of the maxillary tooth morphology varies in the literature, some say that they are comparable to the teeth of *Paraplacodus*, while others describe them as being overall rounded, "subquadrate," or hemispheric (Owen, 1858; Mazin, 1989; Rieppel, 2000). The gross morphology of the palatine teeth is noticeably difference from the maxillary teeth. Palatine teeth are overall larger and are said to vary in size with smaller teeth being more rostral and larger teeth caudal. Palatine teeth take on a more triangular or quadrilateral appearance, as compared to the button-like shape of the maxillary teeth, and are described as being overall flatter (Owen, 1858; Mazin. 1989).

Within the armored cyamodontoids there is further subdivision, between the Placochelyidae and other cyamodontoids (Fig 3.2), which is reflected in changes in dentition. Members of the genus *Cyamodus* have one to two reduced blunted premaxillary teeth, two to three maxillary teeth, and two to three palatine teeth, though tooth counts vary by species and with ontogeny (Fig 3.3c; Mazin, 1989). The description of maxillary teeth in *Cyamodus ssp* ranges from teeth having a full oval crown to being hemispherical (Mazin, 1989; Owen. 1858). Both the maxillary and palatine teeth of *Cyamodus* vary in size within a tooth row, increasing in

size from rostral to caudal, and relative tooth sizes and number can also change with ontogeny (Mazin, 1989). The most rostral palatine teeth resemble the caudal-most maxillary teeth in size and shape, but the caudal-most palatine teeth are much larger and are described as having a full oval, elliptical, or bean shape, with the long axis of the tooth roughly parallel to the line of the maxillary teeth (Mazin, 1989; Neenan, et al, 2014; Owen, 1858).

Within the non-placochelyid cyamodontoids, and sister to *Cyamodus, Henodus* is thought to have deviated from the durophagous lifestyle typical of other placodonts, and instead acted as a filter feeder, eating small branchiopods, or grazer (Huene, 1936; Reif & Stein, 1999, Mazin & Pinna, 1993). *Henodus* has a reduced dentition, with a row of small premaxillary teeth and only a single pair of reduced palatine teeth on each side of the mouth (Fig 3.3d).

Setting them apart from other placodonts, members of the Placochelyidae have lost their premaxillary teeth and instead have developed an elongated rostrum. *Protenodontosaurus*, sister taxon to the placochelyids, has a single pair of premaxillary teeth and there is evidence that this may be a juvenile condition for the placochelyids (Fig 3.3e; Nosotti & Pinna, 1999). Placochelyids typically have 2-3 pairs of maxillary teeth, described as being flat or flattened, which increase in size from rostral to caudal, and two pairs of palatine teeth, the rostral of which is similar to the last maxillary tooth. In the literature, the caudal-most palatine tooth is described as being much bigger than the first palatine tooth, elliptical or ovoid, and is often said to be flat (Fig 3.3f & g; Mazin, 1989). This dental arrangement is sufficiently different from other placodonts that it has led some to believe that placochelyid placodonts were using their rostra to burrow into muddy substrates to find sub-benthic invertebrates, likely bivalves, instead of picking epibenthic invertebrates off of the substrate (Mazin & Pinna, 1993). However, given the

lack of shelly taxa in placochelyid bearing deposits, it has been argued that they may have been preying on epibenthic crustaceans instead (Stefani et al., 1992).

3.1.3 *Institutional Abbreviations*

GPIT, Senckenberg Center for Human Evolution and Palaeoenvironment, Tubingen, Germany; MB.R., Museum für Naturkunde, Berlin, Germany; PIMUZ T , Paläontologisches Institut und Museum der Universität, Zurich, Switzerland; SMNS, Staatliches Museum für Naturkunde, Stuttgart, Germany; MFSN, Museo Friulano di Storia Naturale, Udine, Italy; V, Museo Civico di Storia Naturale, Milan, Italy .

3.2 METHODS AND MATERIALS

To quantify occlusal morphology, I measured the radius of Curvature (RoC) for each tooth (Fig. 3.4). A large RoC would correspond to a flat or very shallow occlusal surface and as the RoC decreases, the tooth would become pointier. Positive RoCs correspond to teeth that have an overall convex morphology, and a negative RoC would indicate a concavity in the occlusal surface. When possible, specimens were scanned with a Next Engine laser scanner (NextEngine Inc., CA) to collect 3D surface data, and RoC was measured using the built-in tool-set in Geomagic (3D Systems Inc., SC) to fit a sphere to the occlusal surface of each tooth, either by highlighting the surface or by placing four points on the surface to be measured (Fig. 3.5). Both approaches worked equally well for simple rounded tooth surface, but for more complex tooth surfaces the four-point approach allowed for more control over the curvature being measured.

In some instances it was not possible to scan specimens, so measurements were taken from photographs using Image J (National Institute of Health, USA) or from 3D surfaces

reconstructed using photogrammetry (Falkingham, 2012). Photos were taken with a Kodak Easyshare camera (Z5120) and 3D models were constructed using VisualSFM (Wu, 2013; Wu, 2011). Only specimens and casts with teeth *in situ* were used for this study.

To better compare gross tooth morphology, tooth RoC was normalized by maximum occlusal cross-sectional diameter. This allowed for comparison between teeth, across taxa, and to canonical models.

3.3 RESULTS

3.3.1 *Paraplacodus broilii*

The average radius of curvature (RoC) of *Paraplacodus boilii* maxillary teeth is 2.1547 mm and varies from 1.9197 mm to 2.378 mm. Palatine teeth were distinguished from maxillary teeth by the lack of a semi-conical cusp and a more rectangular occlusal cross-section. The RoC of palatine teeth varies from 2.1171 mm to 10.6977 mm, but on average is 4.9095 mm (Fig. 3.6a; Table 3.1).

3.3.2 *Placodus ssp*

Placodus teeth, *in situ*, show a typical pattern of wear, with wear facets facing each other: maxillary teeth worn on the lingual size and palatine teeth worn on the labial side. On average, maxillary teeth have a larger RoC (10.0551 mm) than seen in *Paraplacodus broilii* maxillary teeth, ranging from 7.3188 mm to 18.7163 mm. *Placodus* palatine teeth typically have larger RoCs, on average 42.63132 mm, than maxillary teeth, but can range from 18.6613 mm to 95.779 mm (Fig. 3.6b).

3.3.3 *Cyamodus ssp*

The maxillary teeth in *Cyamodus* specimens are relatively small, but have a larger average RoC (14.392 mm) than the maxillary teeth in *Placodus ssp*. The rostral most *Cyamodus* maxillary teeth have smaller RoCs (4.68715- 8.75515 mm) than the caudal most maxillary teeth (7.8553- 16.4264 mm). The average RoC for the palatine teeth of *Cyamodus* is 47.4001 mm, but there is a noticeable disparity between the caudal palatine teeth, and the rostral-most palatine teeth, which often have similar RoCs to the caudal-most maxillary teeth. For the first palatine tooth RoCs range from as low as 5.45075 mm to 30.90705 mm. The caudal-most palatine teeth have the largest RoCs, ranging from 30.9794 mm to 299.5883 mm in magnitude. For most specimens this means that the caudal-most teeth are shallowly convex, however in two specimens, *Cyamodus sp* (SMNS 91472) and *C. rostratus* (MB.R.1773), the caudal-most palatine teeth are shallowly concave, with RoCs ranging from -66.5331 mm to - 299.5883 mm (Fig. 3.6c).

3.3.4 *Protenodontosaurus italicus and the Placochelyidae*

Protenodontosaurus italicus is the sister taxon to the Placochelyidae, and represents a transitional form between other placodonts, with a single pair of premaxillary teeth on an elongated snout. The single pair of maxillary teeth have an average RoC of 16.0065 mm, and vary from 13.8885 mm to19.1968 mm. There are two pairs of palatine teeth for *P. italicus*, and the rostral and caudal teeth differ in size. The rostral-most palatine teeth have an average RoC of 13.6987 mm, varying from 8.584 mm to 20.3792 mm, and are roughly similar in size and shape to the maxillary teeth. The larger, caudal pair of palatine teeth in *P. italicus* have an average RoC of 37.5999 and range from 33.7046 mm to 40.2767 mm (Fig 3.6d).

For this study I measured data from two genera within the Placochelyidae: *Psephoderma alpinum* and *Plachchelys placodonta*, and the teeth of both species followed similar patterns. The rostral portion of one *Placochelys placodonta* specimen (MB.R. 1765) was broken off, so I only have data for the last two maxillary teeth. However, I also have data from a cast of an almost compete *Placochelys placodonta* (cast - MB.R.1767.1) which has all three maxillary teeth. *Psephoderma alpinum* (PIMUZ T), in contrast, has only two maxillary teeth. The first maxillary teeth of *Placochelys placodonta* have a small RoC, 4.7403 mm on the left and 1.15115 mm on the right. Caudal maxillary teeth in all three specimens have RoCs of larger magnitudes, on average 51.5394 mm, but vary between concave (-5.8808 mm to -106.6309 mm) and convex (11.556 mm to 47.0535 mm). In all three specimens there are two pairs of palatine teeth. The rostral palatine teeth are similar to the last pair of maxillary teeth in size and shape, with an average RoC of 13.3772 mm, and can be concave, with RoCs varying from -8.4457 mm to -24.487 mm, or convex in one specimen (MB.R.1765) with RoCs of 12.4456 mm and 12.7255 mm.

The caudal-most palatine teeth in both *Placochelys placodonta* and *Psephoderma alpinum* have a more complex morphology than can be measured with a single RoC (Fig 3.4b). These teeth have a shallow, slightly curved furrow or concavity running the length of the tooth, and on the medial-caudal edge of the concavity there is a small cusp projecting from the occlusal surface. The average RoC of the concavity is – 37.5782 mm and varies from -29.0175mm to -58.5793 mm. The average RoC of the cusp is 7.1682 mm and varies from 4.4033 mm to 9.6845 mm (Fig. 3.6e).

3.4 DISCUSSION

The differences in tooth radius of curvature (RoC) for non-placochelyid placodonts overall agrees with the qualitative descriptions, where conical or rounded teeth give way to more flattened shape, as previously described in the literature (Fig 3.6; Fig 3.7). The maxillary teeth of *Paraplacodus broilii* have the lowest RoC, and are the most similar to the piercing teeth of the sister taxon to the placodonts (Neenan, 2013). The palatine teeth have a larger average RoC than the maxillary teeth, but these teeth are still more pointed than the palatine teeth of other placodonts, though there is some overlap with the RoC of maxillary teeth in other groups. *Placodus ssp* have rounded maxillary teeth, with a larger RoC than the maxillary teeth of *Paraplacodus broilii*, and which would have been less likely to break while still effectively crushing prey. The average RoC of the palatine teeth is much larger than the RoC for the maxillary teeth, approaching the optimal tooth shape. In *Cyamodus ssp*, the rostral maxillary teeth have smaller RoCs, indicating that they may have been less involved with crushing shelled prey. Caudal maxillary teeth, in contrast, have larger RoCs, similar to those measured for the rostral palatine teeth, and were probably moderately involved in breaking prey. The large RoCs of the caudal-most palatine teeth of *Cyamodus ssp* make these most like the 'optimal' tooth predicted by the physical and FEA models. While most of these teeth are shallowly convex, there were two specimens with concave palatine teeth, but the RoCs were sufficiently large to be functionally flat.

One possible reason for this pattern of increasing RoC, specifically comparing *Paraplacodus broilii* and *Placodus ssp,* could be an overall increase in size. *Paraplacodus broilii* was smaller than *Placodus ssp*, and the larger animals would be more likely to have teeth with larger RoCs due to scaling. Using cranial length as a proxy for body size, *Placodus ssp*

(cranial length – 179.979 mm; Rieppel, 1995) are about 1.668 times larger than *Paraplacodus broilii* (cranial length – 107.907 mm; Rieppel, 2000). If tooth RoC were to scale isometrically, then scaled-up *Paraplacodus broilii* teeth (maxillary – 3.5938 mm, palatine – 8.1586 mm) would still have smaller RoCs than *Placodus* for both maxillary and palatine teeth. Similarly, when RoCs are normalized by tooth diameter, *Paraplacodus broilii* still have smaller RoCs than *Placodus sp.*(Fig 3.6a & b).

Contrary to what has been reported in the literature, the palatine teeth of placochelyid placodonts are not flat. Instead, these teeth have a more complex morphology, with a crescent shaped furrow running the length of the tooth and a medial cusp. This would seem to indicate that these organisms do, in fact, have a different dietary specialization than the other placodonts, or have specialized for durophagy in a different way. The shallow concavity may dissipate in-tooth strain, and serve to localize any damage that might occur (Crofts, 2015; Qasim et al., 2004), while the cusp, which has a relatively small RoC, concentrates stress applied to the prey item (Crofts& Summers, 2014). A similar system has been proposed for bunodont molars, where four low cusps hold hard food items in place and disperse in-tooth stress, and a single taller, sharper cusp applies stress to break the shell (Berthaume, 2013).

As has been argued above, the ability of teeth to break shells without breaking themselves is a large part of a predator's success, but to "win" in the predator-prey arms-race, predators must also be able to eat their prey. We know from the late Olenekian brolomites, inferred to be regurgitates of durophagous predators, possibly sharks, colobodontids, pachypleurosaurs, or placodonts, that they were primarily crushing and feeding on bivalves, with some crinoids, gastropods and even some vertebrates represented as well (Salamon et al., 2012). However, not all shelled organisms would be potential prey items, as there is a trade-off between energy

invested in prey-handling and predator success. Thicker shelled or larger animals often present greater resistance to failure than smaller or thinner shelled alternatives, and predators will be more likely to consume or attempt to consume the easier to break prey or prey that required less handling time (Boulding, 1984; Kislalioglu & Gibson, 1976). Placodonts similarly seem to have been limited in what prey they could have processed. For example, based on tooth wear facets, the inferred volume between teeth, and morphology of the lever formed by the mandible, it has been predicted that *Placochelys placodonta* could have eaten prey that was at most 50×25×15mm. Additionally, given the morphology of different crushing surface, *P. placodonta* would have had a minimum prey size of 15×12×10 mm for the small anterior-lateral crushing areas and 35×20×10 mm for the larger medial crushing area involving the caudal-most palatine teeth (Mazin & Pinna, 1993). If bitten prey were not consumed, due to size refugia or some other defensive trait, and experienced only sub-lethal damage, they would have been able to repair their shells and pass along whatever trait or traits allowed them to survive the encounter.

While the advances in shell defenses typically associated with the Mesozoic Marine Revolution (MMR; Vermeij, 1977) have traditionally been described as occurring in the Jurassic and accelerating in the Cretaceous, more recent work indicates that these selective pressures may have begun earlier. Toothed hinges and cementing to substrates, for example, appear in the Carnian (Vermeij, 2008), when we see the greatest diversity of Placodonts, and brachiopod defensive ornamentation also increases throughout the Triassic (Vörös, 2010). While environmental factors that may have also driven changes in shelled prey, such as competition for space or environmental stability leading to increased infaunalization in Triassic bivalves (McRoberts, 2001), these changes would have also lead to new challenges for predators.

Placodus sp have been found in deposits with a diversity of shelly invertebrate taxa, including moderately mobile/shallowly burrowing bivalves and crinoids, known to be part of Triassic durophagous predator diets, as well as brachiopods, asteroids, ophiuroids, gastropods (Assmann, 1937; Salamon et al., 2012). *Cyamodus sp* and *Placodus sp* can also co-occur in later deposits, and are found with some of the same bivalves, ophiuroids, and asteroids as seen in *Placodus sp* deposits (Blake & Hagdorn, 2003).

With bivalves increasingly burrowing into the substrate through the Triassic (McRoberts, 2001), later occurring groups of placodonts may have needed different approached obtaining prey. There is some evidence that the Cyamodontoid lineage may have been capable of creating suction to pull in water, either for feeding, as was likely in the case of *Henodus*, or for olfaction (Rieppel, 2002). Within the Cyamodontoid group, the placochelyids have been postulated to have occupied the same ecological niche as modern rays, using their rostrum and/or buccal suction to root-out increasingly common infaunal bivalves (Rieppel, 2002). However, placochelyids appear in deposits that seem to lack bivalves, with rare instances of gastropod and echinoderm taxa, but instead seem to be dominated by epifaunal decapod crustaceans (Stefani, et al., 1992).

Given the potential differences in diet, one might expect to see variation in bite-force across the phylogeny which could also help explain differences in tooth morphology. A durophagous diet requires high bite forces to induce failure in hard-shelled prey items, and in modern taxa we see features like enlarged sites for jaw muscle attachment and modifications to increase mechanical advantage of the jaws in durophagous lizards (Dalrymple, 1979). Inferred muscle attachments, in both the placodontoids and cyamodontoids, indicate the there was a division of labor in jaw closing: the mechanical advantage of the jaw adductors would have been greatest at

small gapes, whereas at wider gape angles pterygoideus muscles would have provided the most power. It is likely that these two sets of muscles worked together, depending on the size of the prey item. Additionally the huge superficial pterygoideus may have helped prevent disarticulation of the mandible during strong bites (Rieppel 2002). In addition to the stabilization provided by the pterygoideus muscles, placochelyids may have been able to use their elongate rostrum to dissipate twisting forces resulting from high bite forces. Similarly, non-placochelyid cyamodontoids could have also dissipated forces, to lesser extent, in their short snouts (Mazin & Pinna, 1993).

Given the ability to generate high bite forces, there is an increased emphasis on the functional size of teeth in durophagous taxa: increasing the size of teeth while decreasing their number, and decreasing the overall replacement rate to maximize the number of functional teeth at any one time (Dalrymple, 1979). In placodonts, from the placodontoids to the cyamodontoids and placochelyids, we see an overall decrease in tooth number (Mazin, 1989) as well as increasing RoCs that reduce the likelihood of tooth failure. There is also an overall pattern of decreased tooth replacement rates in cyamodontoid lineages compared to placodontoids. Moreover, tooth replacement becomes more organized in the cyamodontoids, with placochelyids replacing teeth infrequently and so that there is always one functional crushing surface at any one time (Fig 3.6; Neenan, 2014).

While function is not the only factor dictating tooth morphology, the pattern of change across the placodont lineage indicates that the trade-off between breaking prey items while maintaining tooth integrity may influence morphology. In addition to the changes seen in tooth number, replacement, and occlusal morphology, tooth material composition may also change in response to changes in diet, as thicker enamel is better able to resist deformation under high

loads than thin, worn enamel (Lucas et al., 2008). Similarly, I have only addressed changes in teeth of the upper jaw, but these interact with similarly shaped teeth in the lower jaw, the morphology of which will affect how prey items are loaded. This study is a first step in understanding the larger pattern of how tooth morphology changes with the shift to a durophagous diet within a single lineage.

3.5 TABLES AND FIGURES

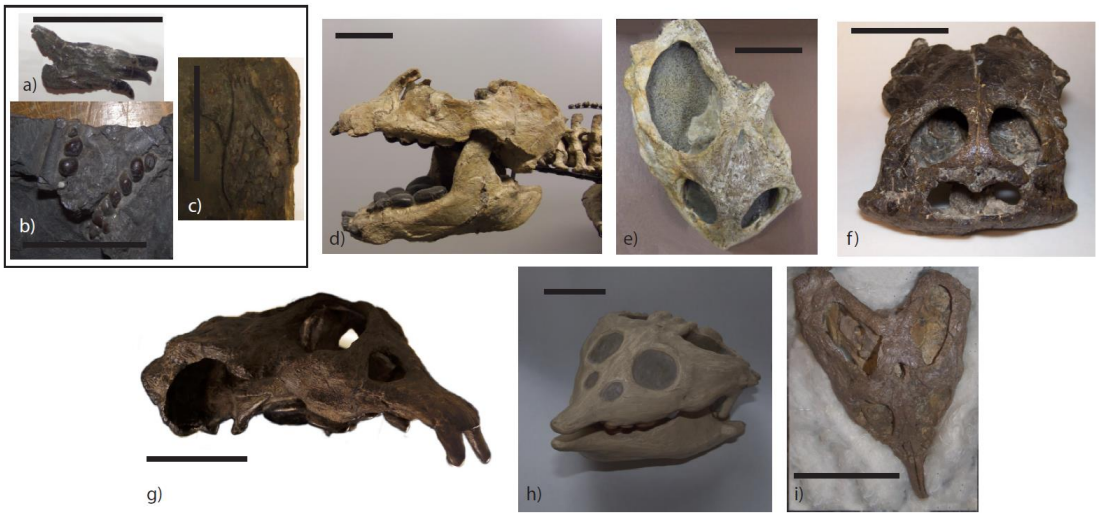

Figure 3.1 - Placodont diversity. *Paraplacodus broilii* premaxilla (a; PIMUZ T 4773), maxillary teeth (b; PIMUZ T 4776), and ventral view of dentaries and palatine teeth (c; PIMUZ T 2805) d) *Paraplacodus gigas* e) Cya*modus sp* (SMNS 91472) f) *Henodus chelyops* (GPIT/RE/7289) g) *Protenodontosaurus italicus* (MFSN 1819) h) cast of *Placochelys placodonta* (MB.R. 1767.1) h) *Psephoderma alpinum* (V. 471). All scale bars are 5 mm.

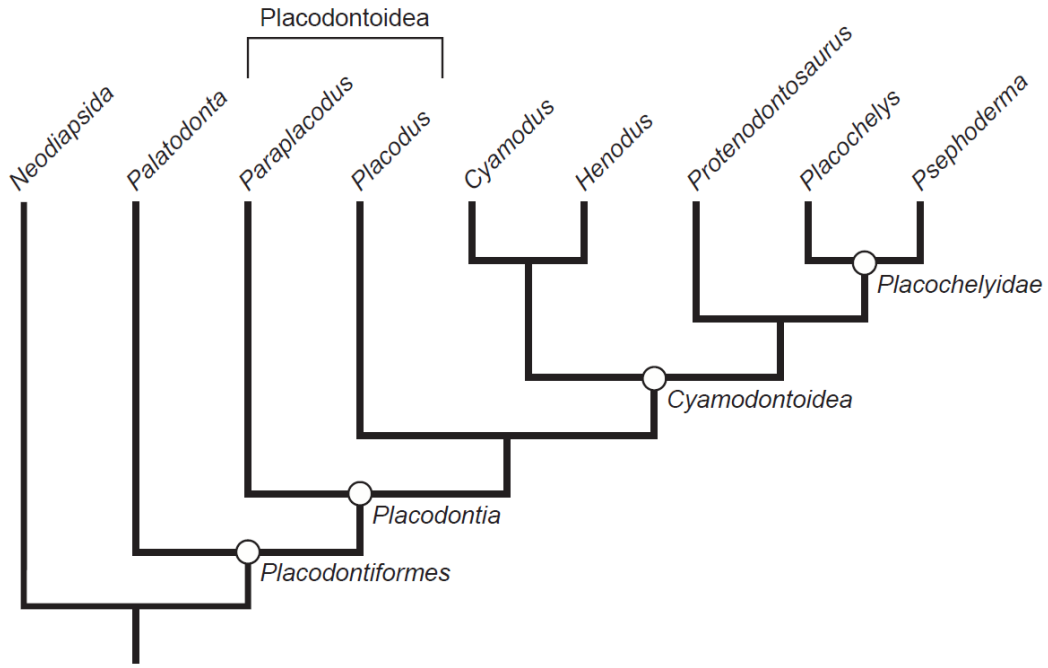

Figure 3.2 - Tree showing the phylogenetic relationships between the Placodontiformes. Major groups labeled at nodes (if monophyletic) or with brackets above tree (if paraphyletic). Modified from Neenan et al.(2014).

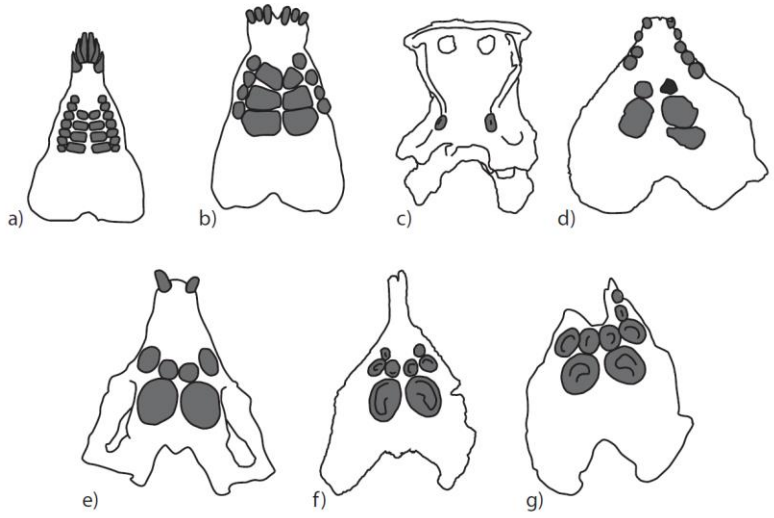

Figure 3.3 - Diversity of Placodont tooth arrangement, size and morphology. a) *Paraplacodus broilii* b) *Placodus gigas* as a representative *Placodus sp* c) *Cyamodus hildegardis*, as a representative *Cyamodus sp* d) *Henodus chelyops* e) *Protenodontosaurus italicus* f) *Placochelys placodonta* f) *Psephoderma alpinum*.

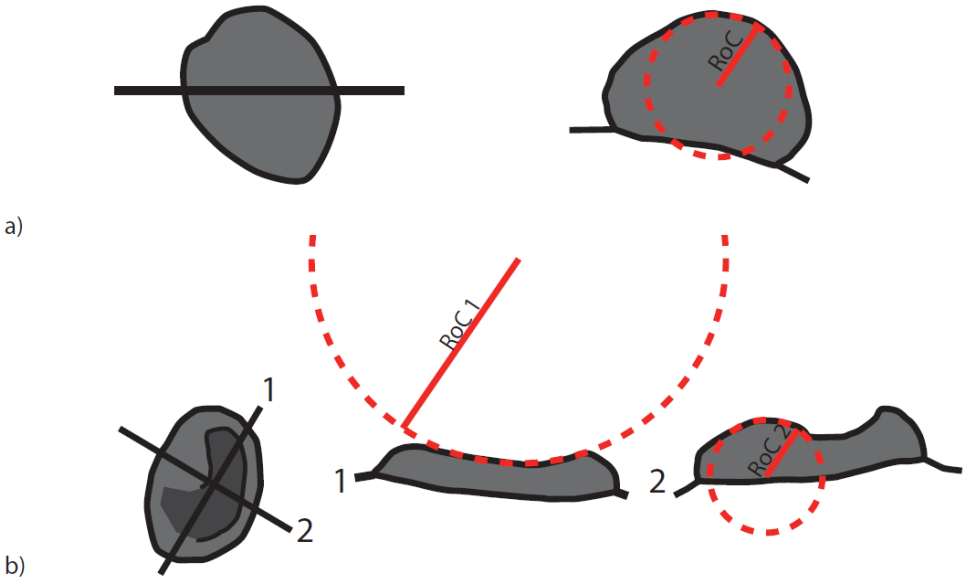

Figure 3.4 - Diagram of Radius of Curvature (RoC) measurements for teeth with a single occlusal curve (a) and for more complex teeth (b). Circles (in dashed red lines) are fit to the occlusal curvature of the tooth, and the radius (solid red line) is measured.

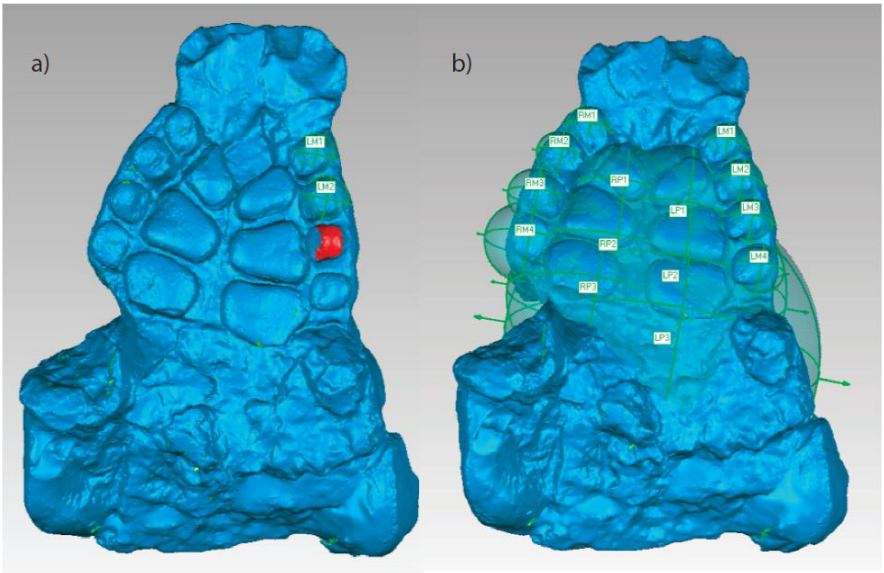

Figure 3.5 - Fitting spheres to tooth occlusal surfaces with Geomagic. a) Occlusal surfaces are fit to portions of the highlighted in red. b) Example of spheres fit to all maxillary and palatine teeth of *Placodus gigas*.

*

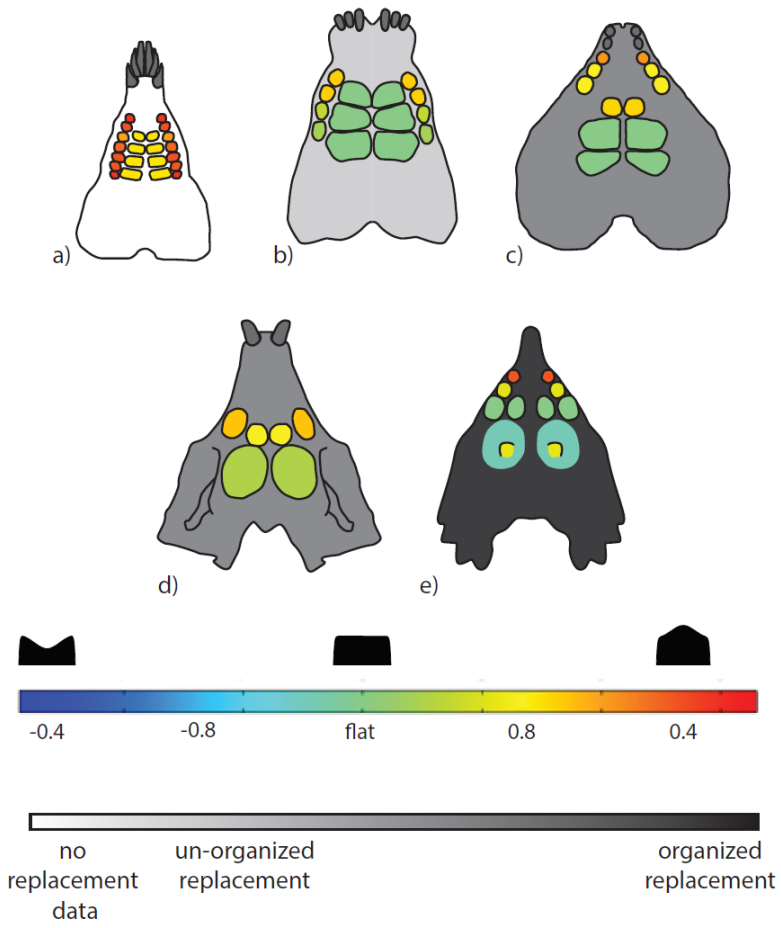

Figure 3.6 - Comparison of placodont tooth radius of curvature (RoC) between teeth and across taxa. RoC for each tooth is normalized by maximum diameter of the tooth to allow for comparison between individual teeth, between taxa, and with canonical models. Teeth are color coded by RoC with warmer colors representing small but positive RoCs, green teeth are approximately flat, and cooler colors represent negative RoCs. Skull outlines are color coded to demonstrate degree of organization in tooth replacement. *Paraplacodus* is white to indicate that there is no information for this taxon. Light grey indicates taxa where there a faster, less organized tooth replacement and darker grey indicates more organized, slower tooth replacement.

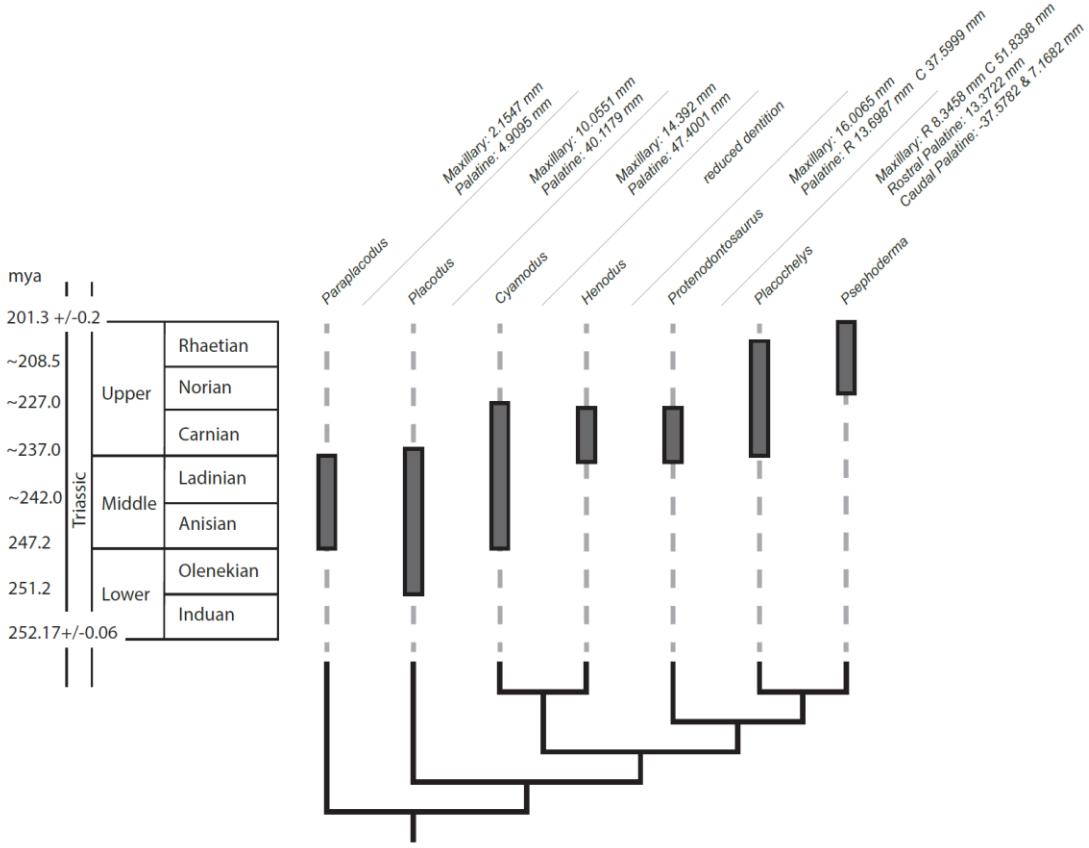

Figure 3.7 - Tree showing placodont relationships correlated with occurrence of each taxon and tooth radius of curvature (RoC) data. Grey bars span time during which taxa occurred, and the tree structure is not correlated to time. For each Genus, average tooth RoC is given for maxillary teeth and palatine teeth, except *Henodus* which had a highly reduced dentition, ostensibly for filter feeding, and the Placochlyids (*Placochelys* and *Psephoderma*) which are averaged together. Two measurements are included if there is a difference in tooth RoC between rostral (R) and caudal (C) teeth. In the Placochelyids the rostral and caudal palatine tooth RoCs are reported separately because the more complex morphology of the caudal palatine tooth requires two RoCs for the tooth concavity (-37.5782 mm) and medial cusp (7.1682 mm).

Table 3.1 - Tooth measurements by species with specimen number and method of data collection

Species	Specimen Number	Side	Tooth type	tooth number	Primary RoC (mm)	Secondary RoC (mm)	Data used
Paraplacodus broilii	PIMUZ T 4776			max A	2.05585	NA	Laser scan, Geomagic
				max B	1.9197	NA	Laser scan, Geomagic
				max C	2.2653	NA	Laser scan, Geomagic
				Pal D	4.63745	NA	Laser scan, Geomagic
				Pal E	10.6977	NA	Laser scan, Geomagic
				max F	2.378	NA	Laser scan, Geomagic
	PIMUZ T 2805	Left	Palatine	2	2.1171	NA	Laser scan, Geomagic
		Left	Palatine	4	4.34055	NA	Laser scan, Geomagic
		Right	Palatine	1	8.9568	NA	Laser scan, Geomagic
		Right	Palatine	3	3.59175	NA	Laser scan, Geomagic
		Right	Palatine	4	2.5567	NA	Laser scan, Geomagic
Placodus sp	SMNS - no number	Right	Maxillary	1	7.48635	NA	Laser scan, Geomagic
		Right	Maxillary	2	13.4504	NA	Laser scan, Geomagic
		Right	Maxillary	3	18.7163	NA	Laser scan, Geomagic
		Left	Palatine	1	34.21475	NA	Laser scan, Geomagic
		Left	Palatine	2	70.32245	NA	Laser scan, Geomagic
		Left	Palatine	3	46.13785	NA	Laser scan, Geomagic
		Right	Palatine	1	31.04565	NA	Laser scan, Geomagic

		Right	Palatine	2	95.7799	NA	Laser scan, Geomagic
		Right	Palatine	3	38.23145	NA	Laser scan, Geomagic
	SMNS - no number	Left	Maxillary	1	12.812	NA	Laser scan, Geomagic
		Left	Maxillary	2	7.4171	NA	Laser scan, Geomagic
		Left	Maxillary	3	14.9503	NA	Laser scan, Geomagic
		Right	Maxillary	1	7.05665	NA	Laser scan, Geomagic
		Right	Maxillary	2	8.7788	NA	Laser scan, Geomagic
		Right	Maxillary	3	7.3188	NA	Laser scan, Geomagic
		Right	Maxillary	4	11.3352	NA	Laser scan, Geomagic
		Left	Palatine	1	22.9802	NA	Laser scan, Geomagic
		Left	Palatine	2	29.15575	NA	Laser scan, Geomagic
		Right	Palatine	1	38.17405	NA	Laser scan, Geomagic
		Right	Palatine	2	28.63535	NA	Laser scan, Geomagic
	SMNS 392	Left	Maxillary	1	7.7014	NA	Laser scan, Geomagic
		Left	Maxillary	2	8.5603	NA	Laser scan, Geomagic
		Left	Maxillary	3	8.2825	NA	Laser scan, Geomagic
		Left	Maxillary	4	9.6957	NA	Laser scan, Geomagic
		Right	Maxillary	1	8.2634	NA	Laser scan, Geomagic
		Right	Maxillary	2	8.6886	NA	Laser scan, Geomagic
		Right	Maxillary	3	10.3375	NA	Laser scan, Geomagic
		Right	Maxillary	4	15.41655	NA	Laser scan, Geomagic
		Left	Palatine	1	29.7014	NA	Laser scan,

		Left	Palatine	2	44.18065	NA	Geomagic Laser scan, Geomagic
		Left	Palatine	3	60.1148	NA	Geomagic Laser scan, Geomagic
		Right	Palatine	1	18.6613	NA	Geomagic Laser scan, Geomagic
		Right	Palatine	2	30.60005	NA	Geomagic Laser scan, Geomagic
		Right	Palatine	3	30.99055	NA	Geomagic Laser scan, Geomagic
Placodus gigas	SMNS 59434	Right	Maxillary	1	7.7693	NA	Geomagic Laser scan, Geomagic
		Right	Maxillary	2	8.0643	NA	Geomagic Laser scan, Geomagic
		Right	Maxillary	3	10.6608	NA	Geomagic Laser scan, Geomagic
		Right	Maxillary	4	8.45075	NA	Geomagic Laser scan, Geomagic
		Right	Palatine	1	33.07815	NA	Geomagic Laser scan, Geomagic
		Right	Palatine	2	42.7057	NA	Geomagic Laser scan, Geomagic
		Right	Palatine	3	47.05355	NA	Geomagic Laser scan, Geomagic
Cyamodus hildegardis	PIMUZ T 4768	Left	Maxillary	1	11.54045	NA	Geomagic Laser scan, Geomagic
		Left	Maxillary	2	6.8391	NA	Geomagic Laser scan, Geomagic
		Left	Maxillary	3	7.8553	NA	Geomagic Laser scan, Geomagic
		Right	Maxillary	2	7.08185	NA	Geomagic Laser scan, Geomagic
		Right	Maxillary	3	13.6074	NA	Geomagic Laser scan, Geomagic
		Left	Palatine	2	27.37335	NA	Geomagic Laser scan, Geomagic
		Left	Palatine	3	30.9794	NA	Geomagic Laser scan, Geomagic
		Right	Palatine	1	15.0135	NA	Geomagic Laser scan, Geomagic
Cyamodus rostratus	MB.R.1773	Left	Maxillary	1	8.6559	NA	Geomagic Laser scan, Geomagic
		Left	Maxillary	2	11.90875	NA	Laser scan,

		Left	Maxillary	3	11.2595	NA	Geomagic Laser scan,
		Right	Maxillary	1	5.01185	NA	Geomagic Laser scan,
		Right	Maxillary	2	5.3428	NA	Geomagic Laser scan,
		Right	Maxillary	3	11.6396	NA	Geomagic Laser scan,
		Left	Palatine	1	13.16925	NA	Geomagic Laser scan,
		Left	Palatine	2	-299.588	NA	Geomagic Laser scan,
		Right	Palatine	1	12.6976	NA	Geomagic Laser scan,
		Right	Palatine	2	-125.737	NA	Geomagic Laser scan,
Cyamodus munsteri	MB.R.1774 - cast	Left	Maxillary	1	6.00425	NA	Geomagic Laser scan,
		Left	Maxillary	2	11.1497	NA	Geomagic Laser scan,
		Right	Maxillary	1	4.68715	NA	Geomagic Laser scan,
		Right	Maxillary	2	5.87675	NA	Geomagic Laser scan,
		Left	Palatine	1	30.90705	NA	Geomagic Laser scan,
		Left	Palatine	2	7.86455	NA	Geomagic Laser scan,
		Left	Palatine	3	38.663	NA	Geomagic Laser scan,
		Right	Palatine	1	5.45075	NA	Geomagic Laser scan,
		Right	Palatine	2	6.64035	NA	Geomagic Laser scan,
		Right	Palatine	3	38.7477	NA	Geomagic Laser scan,
Cyamodus laticeps	SMNS 54028	Left	Maxillary	1	5.8045	NA	Geomagic Laser scan,
		Left	Maxillary	2	12.02185	NA	Geomagic Laser scan,
		Left	Maxillary	3	11.28295	NA	Geomagic Laser scan,
		Right	Maxillary	1	4.77695	NA	Geomagic Laser scan,

		Right	Maxillary	3	10.9136	NA	Geomagic Laser scan, Geomagic
		Left	Palatine	1	12.8405	NA	Laser scan, Geomagic
		Left	Palatine	2	67.36405	NA	Laser scan, Geomagic
		Right	Palatine	2	85.7624	NA	Laser scan, Geomagic
Cyamodus sp	SMNS 15855	Left	Maxillary	2	16.4264	NA	Laser scan, Geomagic
		Right	Maxillary	1	8.75515	NA	Laser scan, Geomagic
		Right	Palatine	1	15.48615	NA	Laser scan, Geomagic
		Right	Palatine	2	106.156	NA	Laser scan, Geomagic
Cyamodus sp	SMNS 17403	Left	Palatine	1	10.9054	NA	Laser scan, Geomagic
		Left	Palatine	2	70.8695	NA	Laser scan, Geomagic
		Right	Palatine	1	7.4569	NA	Laser scan, Geomagic
Cyamodus sp.	SMNS 91472	Left	Maxillary	2	9.27285	NA	Laser scan, Geomagic
		Right	Maxillary	1	5.31225	NA	Laser scan, Geomagic
		Right	Maxillary	2	7.85815	NA	Laser scan, Geomagic
		Left	Palatine	1	8.5251	NA	Laser scan, Geomagic
		Left	Palatine	2	-72.5881	NA	Laser scan, Geomagic
		Right	Palatine	1	7.6828	NA	Laser scan, Geomagic
		Right	Palatine	2	-66.5331	NA	Laser scan, Geomagic
Protenodontosaurus italicus	MFSN 1923 GP	Left	Maxillary	1	14.93426	NA	Image J/ Photo
		Left	Palatine	1	15.2046	NA	Image J/ Photo
		Left	Palatine	2	37.96985	NA	Image J/ Photo
		Right	Palatine	1	20.37917	NA	Image J/ Photo
		Right	Palatine	2	33.70461	NA	Image J/ Photo

Protenodontosaurus italicus	MFSN 1819 GP	Left	Maxillary	1	19.1968	NA	Image J/ Photo
		Right	Maxillary	1	13.88854	NA	Image J/ Photo
		Left	Palatine	1	8.583992	NA	Image J/ Photo
		Left	Palatine	2	38.4483	NA	Image J/ Photo
		Right	Palatine	1	10.62718	NA	Image J/ Photo
		Right	Palatine	2	40.2767	NA	Image J/ Photo
Psephoderma alpinum	PIMUZ T - no number	Left	Maxillary	1	-5.88075	NA	Laser scan, Geomagic
		Left	Maxillary	2	-14.5389	NA	Laser scan, Geomagic
		Right	Maxillary	1	-9.38225	NA	Laser scan, Geomagic
		Right	Maxillary	2	-8.7272	NA	Laser scan, Geomagic
		Left	Palatine	1	-24.487	NA	Laser scan, Geomagic
		Left	Palatine	2	-33.3342	8.8169	Laser scan, Geomagic
		Right	Palatine	1	-10.41	NA	Laser scan, Geomagic
		Right	Palatine	2	-33.488	6.7389	Laser scan, Geomagic
Placochelys placodonta	MB.R.1765	Left	Maxillary	1	-15.5651	NA	Laser scan, Geomagic
		Left	Maxillary	2	-98.3232	NA	Laser scan, Geomagic
		Right	Maxillary	2	-106.631	NA	Laser scan, Geomagic
		Left	Palatine	1	12.7255	NA	Laser scan, Geomagic
		Left	Palatine	2	-29.0175	9.6845	Laser scan, Geomagic
		Right	Palatine	1	12.44555	NA	Laser scan, Geomagic
		Right	Palatine	2	-58.5793	7.61115	Laser scan, Geomagic
Placochelys placodonta	MB.R.1767.1 - cast	Left	Maxillary	1	4.7403	NA	Laser scan, Geomagic
		Left	Maxillary	2	-10.145	NA	Laser scan, Geomagic
		Left	Maxillary	3	47.0535	NA	Laser scan,

	Right	Maxillary	1	1.15115	NA	Geomagic Laser scan, Geomagic
	Right	Maxillary	2	11.55595	NA	Geomagic Laser scan, Geomagic
	Right	Maxillary	3	35.76465	NA	Geomagic Laser scan, Geomagic
	Left	Palatine	1	-8.4457	NA	Geomagic Laser scan, Geomagic
	Left	Palatine	2	-31.4331	5.7546	Geomagic Laser scan, Geomagic
	Right	Palatine	1	-11.7196	NA	Geomagic Laser scan, Geomagic
	Right	Palatine	2	-39.6175	4.4033	Geomagic Laser scan, Geomagic

BIBLIOGRAPHY

1 Abler, W. J. 1992 The serrated teeth of tyrannosaurid dinosaurs, and biting structures in other animals. *Paleobiology* 18 161-183.

2 Anderson, P. S. L. 2009 The effects of trapping and blade angle of notched dentitions on fracture of biological tissues. *J Exp Biol* 212, 3627-3632. (DOI 10.1242/jeb.033712)

3 Anderson, P. S. L., Gill, P. G., and Rayfield, E. J. 2011 Modeling the effects of cingula structure on strain patterns and potential fracture in tooth enamel. *J Morph* 272, 50-65.

4 Anderson, P. S. L. & LaBarbera, M. 2008 Functional consequences of tooth design: effects of blade shape on energetics of cutting. *J Exp Biol* 211, 3619-3626. (DOI 10.1242/jeb.020586)

5 Anderson, P. S. L. and Rayfield, E. J. 2012 Virtual experiments, physical validation: dental morphology at the intersection of experiment and theory. *J R Soc Interface* 9, 1846-1855.

6 Assmann, P. 1937 Revision der Fauna der Wirbellosen der oberschlesischen Trias. *Abhandlung der Preussischen Geologischen Landesanstalt* 170:1-126.

7 Berthaume, M., Gross, I. R., Patel, N. D., Strait, D.S., Wood, S. and Richmond, B. G. 2011. The effect of early hominin occlusal morphology on the fracturing of hard food items. *Anat Rec* 293, 594-606.

8 Berthaume, M. A., Dumont, E. R., Godfrey, L. R., and Grosse, I. R. 2013 How does tooth cusp radius of curvature affect brittle food item processing? *J R Soc Interface* 10, 20130240.

9 Berthaume, M. A., Dumont, E. R., Godfrey, L. R., and Grosse, I. R. 2014 The effects of relative food item size on optimal tooth cusp sharpness during brittle food item processing. *J R Soc Interface* 11, 20140965.

10 Blake, D. B. and Hagdorn, H. 2003 The Asteroidea (Echinodermata) of the Muschelkalk (Middle Triassic of Germany). *Paläontologische Zeitschrift* 77(1), 23-58.

11 Boulding, E. G. 1984 Crab-resistant features of shells of burrowing bivalves: decreasing vulnerability by increasing handling time *J Exp Mar Biol Ecol* 76, 201-223.

12 Crofts, S.B. 2015 Finite element modelling of occlusal variation in durophagous tooth systems. *J Exp Biol* (DOI 10.1242/jeb.120097).

13 Crofts, S. B., and Summers, A. P. 2014 How to best smash a snail: the effect of tooth shape on crushing load. *J R Soc Interface* 11, 20131053.

14 Dalrymple, G. H. 1979 On the jaw mechanism of the snail-crushing lizards, Dracaena Daudin 1802 (Reptilia, Lacertilia, Teiidae). *J Herpetol* 13 (3), 303-311.

15 Diedrich, C. G. 2011 Fossil middle Triassic "sea cows" – placodont reptiles as macroalgaw feeders along the north-western Tethys coastline with Pangaea and in the Germanic Basin. *Nat Sci* 3 (1), 9-27.

16 Dumont, E. R., Grosse, I. R., and Slater, G. J. 2009 Requirements for comparing the performance of finite element models of biological structures. *J Theor Biol* 256, 96-103.

17 Enax, J., Prymak, O., Raabe, D. and Epple, M. 2012 Structure, composition, and mechanical properties of shark teeth. *J Struct Biol* 178, 290-299.

18 Evans, A.R. & Sanson, G.D. 2003 The tooth of perfection: functional and spatial constraints on mammalian tooth shape. *Biol J Linn Soc* 78, 173-191. (DOI 10.1046/j.1095-8312.2003.00146.x

19 Evans, A.R. & Sanson, G.D. 2006 Spatial and functional modelling of carnivore and insectivore molariform teeth. *J Morphol* 267, 649-662. (DOI 10.1002/jmor.10285)

20 Falkingham, P. L. 2012 Acquisition of high resolution three-dimensional models using free, open-source, photogrammetric software. *Palaeontol Electron* 15: 1T-15p

21 Ford, C., Bush, M. and Lawn, B. 2009 Effect of wear on stress distributions and potential fracture in teeth. *J Mater Sci: Mater Med* 20, 2243-2247.

22 Freeman, P. W. and Lemen C.A. 2007 The trade-off between tooth strength and tooth penetration: predicting optimal shape of canine teeth. *J Zool* 273, 273-280.

23 Huene, Fv. 1936 *Henodus chelyops*, ein neuer. *Placodontier. Palaeontographica A* 84, 99-148.

24 Kelley, N. P. & Motani, R. 2015 Trophic convergence drives morphological convergence in marine tetrapods. *Biol Lett* 11, 20140709. (DOI 10.1098/rsbl.2014.0709)

25 Keown, A. J., Bush, M. B., Ford, C., Lee, J. J.-W., Constantino, P. J. and Lawn, B.R. 2012 Fracture susceptibility of worn teeth. *J Mech Behav Biomed* 5, 247-256.

26 Kislalioglu, M. and Gibson, R. N. 1976 Prey 'handling time' and its importance in food selection by the 15-spined stickleback, *Spinachia spinachia* (L.). *J Exp Mar Biol Ecol* 25: 115-158.

27 Lawn, B. R. and Lee, J. J-W. 2009 Analysis of fracture and deformation modes in teeth subjected to occlusal loading. *Acta Biomater* 5, 2213-2221.

28 Lawn, B. R., Bush, M.B., Barani, A., Constantino, P. J. and Wroe, S. 2013 Inferring biological evolution from fracture patterns in teeth. *J Theor Biol* 338, 59-65.

29 Lee, J. J.-W., Constantino, P. J., Lucas, P. W. & Lawn, B. R. 2011 Fracture in teeth—a diagnostic for inferring bite force and tooth function. *Biol Rev* 86, 959-974. (DOI 10.1111/j.1469-185X.2011.00181.x)

30 Lucas,. P., Constantino, P., Wood, B. and Lawn, B. 2008 Dental enamel as a dietary indicator in mammals. *Bioessays* 30: 374-385.

31 Luke, D.A & Lucas, P. W. 1983 The significance of cusps. *J Oral Rehabil* 10, 197-206.

32 Mara, K.R., Motta, P. J. and Huber, D. R. 2010 Bite force and performance in the durophagous bonnethead shark, *Sphyrna tiburo*. *J Exp Zool Part A* 313A, 95-105.

33 Massare, J. A. 1987 Tooth morphology and prey preference of Mesozoic marine reptiles. *J Vertebr Paleontol* 7, 121-137. (DOI 10.1080/02724634.1987.10011647)

34 Mazin, J.-M.. 1989 La denture et la region palatine des Placodontia (Reptilia, Trias). Implications phylogénétiques. *Geobios* 22:6, 725-734.

35 Mazin, J. M. & Pinna, G. 1993 Palaeoecology of the armoured placodonts. *Paleontologia Lombarda* 2, 83-91.

36 McRoberts, C. A. 2001 Triassic bivalves and the initial marine Mesozoic revolution: a role for predators? *Geology* 29(4): 359-362.

37 Mehta, R. S. 2009 Ecomorphology of the moray bite: relationship between dietary extremes and morphological diversity. *Physiol Biochem Zool* 82, 90-103.

38 Neenan, J. M., Klein, N., Scheyer, T. M. 2013 European origin of placodont marine reptiles and the evolution of crushing dentition in Placodontia. *Nat Commun* 4, 1621. (DOI 10.1038/ncomms2633)

39 Neenan, J. M., Li, C., Rieppel, O., Bernardini, F., Tuniz, C., Muscio, G & Scheyer, T. M. 2014 Unique method of tooth replacement in durophagous placodont marine reptiles, with new data on the dentition of Chinese taxa. *J Anat* 224(5), 603-613. (DOI 10.1111/joa.12162)

40 Neenan, J. M., Li, C. Rieppel, O. & Scheyer, T. M. 2015 The cranial anatomy of Chinese placodonts and the phylogeny of Placodontia (Diapsida: Sauropterygia). *Zool J Linn Soc Lond* (DOI 10.1111/zoj.12277).

41 Nobiling, G. 1977 Die biomechanik des kieferapparates beim stierkofhai (*Heterodontus portusjacksoni=Heterodontus philippi*). *Adv Anat Embryol Cell Biol* 52, 1-52.

42 Norton, S. F. 1988 Role of the gastropod shell and operculum in inhibiting predation by fishes. *Science* 241, 92-94.

43 Nosotti, S. & Pinna, G. 1999 Skull anatomy of *Protenodontosaurus itallicus* Pinna 1990 (Reptilia, Placodontia). *Paleontologia Lombard* 11, 3-17.

44 Owen 1858 Description of the skull and teeth of the *Placodus laticeps*, Owen, with indications of other new species of *Placodus*, and evidence of the Saurian nature of that Genus. *Philos T Roy Soc* 148, 169-184.

45 Preuschoft, H., Reif, W.-E. and Müller, W. H. 1974 Funktionsanpassungen in form und struktur an haifischzähnen. *Z Anat Entwickl-Gesch* 143, 315-344.

46 Qasim, T., Bush, M. B., Hu, X. and Lawn, B. R. 2005 Contact damage in brittle coating layers: influence of surface curvature. *J Biomed Mater Res B* 73B, 179-185. (DOI 10.1002/jbm.b.30188)

47 Qasim, T., Ford, C., Bush, B.B., Hu, X., Malament, K. A. and Lawn, B.R. 2007 Margin failures in brittle dome structures: relevance to failure of dental crowns. *J Biomed Mater Res B* 80B, 78-85.

48 Ramsay, J. B. and Wilga, C. D. 2007 Morphology and mechanics of the teeth and jaws of white-spotted bamboo sharks (*Chiloscyllium plagiosum*). *J Morph* 268, 664-682.

49 Rieppel, O. 2000 *Paraplacodus* and the phylogeny of the Placodontia (Reptilia: Sauropterygia). *Zool J Linn Soc Lond* 130, 635-659. (DOI 10.1006/zjls.2000.0232)

50 Rieppel, O. 1995 The Genus *Placodus*: Systematics, morphology, paleobiogeography, and paleobiology. *Fieldiana: Geol* 31, 1-44.

51 Rieppel, O. 2002 Feeding mechanics in Triassic stem-group sauropterygians: the anatomy of a successful invasion of Mesozoic seas. *Zool J Linn Soc Lond* 135, 33-63.

52 Reif, W. E. and Stein, F. 1999 Morphology and function of the dentition of *Henodus chelyops* (Huene, 1936) (Placodontia, Triassic). *Newes Jahrbuch für Geologie und Paläontologie, Monatshefte* 1999: 65-80.

53 Salamon, M. A., Niedźwiedzki, R., Przemysław, G., Lach, R. and Surmik, D. 2012 Brolomites from the middle Triassic of Poland and the rise of the Mesozoic marine revolution. *Palaeogeogr Pakaeocl* 321-322: 142-150.

54 Sander, P.M. 2000 Prismless enamel in amniotes: terminology, function, and evolution. In *Development, function and evolution of teeth* (ed. M. F. Teaford, M. M. Smith & W. W. J. Ferguson), 92-106. Cambridge University Press, Cambridge.

55 Sasko, D. E., Dean, M. N., Motta, P. J. & Hueter, R. E. 2006 Prey capture behavior and kinematics of the Atlantic cownose ray, *Rhinoptera bonasus*. *Zoology* 109, 171-181. (DOI 10.1016/j.zool.2005.12.005)

56 Schulp, A. S. 2005 Feeding the mechanical mosasaur: what did Carinodens eat? *Neth J Geosci* 84 345-357.

57 Stefani, M., Arduini, P., Garassino, A., Pinna, G., Teruzzi and G., Trombetta, G. L. 1992 Paleoennviroment of extraordinary fossil biotas from the Upper Triassic of Italy. *Atti della Società Italiana di Scienze Naturale di Milano* 132: 309-335.

58 Summers, A. P. 2000 Stiffening the stingray skeleton – an investigation of durophagy in mylobatid stingrays (Chondrichthyes, Batoidea, Myliobatidae). *J Morphol* 243, 113-126.

59 Van Valkenburgh, B. and Ruff, C. B. 1987 Canine tooth strength and killing behaviour in large carnivores. *J Zool* 212, 379-397.

60 Vermeij, G. J. 1977 The Mesozoic marine revolution: evidence from snails, predators and grazers. *Paleobiology* 3, 245-258.

61 Vermeij, G. J. 2008 Escalation and its role in Jurassic biotic history. *Palaeogeogr Pakaeocl* 263(1-2), 3-8

62 Vörös, A. 2010 Escalation reflected in ornamentation and diversity history of brachiopod clades during the Mesozoic marine revolution. *Palaeogeogr Pakaeocl* 291(3-4), 474-480.

63 Whitenack, L. B. & Motta P. J. 2010 Performance of shark teeth during puncture and draw: implications for the mechanics of cutting. *Biol J Linn Soc* 100, 271-286. (DOI 10.1111/j.1095-8312.2010.01421.x)

64 Whitenack, L. B., Simkins, D. C., Motta, P. J., Hirai, M. & Kumar, A. 2010 Young's modulus and hardness of shark tooth biomaterials. *Arch Oral Biol* 55, 203-209.

65 Whitenack, L. B., Simkins, D. C. Jr and Motta, P. J. 2011 Biology meets engineering: the structural mechanics of fossil and extant shark teeth. *J Morph* 272, 169-179.

66 Wilga, C. D. and Motta, P. J. 2000 Durophagy in sharks: feeding mechanics of the hammerhead *Sphyrna tiburo*. *J Exp Biol* 203, 2781-2796.

67 Wu,C. 2011 Towards Linear-time Incremental Structure From Motion. *3DV*

68 Wu, C., Agarwal, S., Curless, B. and Steven M. Seitz. 2011Multicore Bundle Adjustment. *CVPR*

69 Zuschin, M. & Stanton, R. J. 2001 Experimental measurement of shell strength and its taphonomic interpretation. *Palaios* 16, 161-170. (DOI 10.1669/0883-1351(2001)016<0161:EMOSSA>2.0.CO;2)

VITA

Education:

Undergraduate:
University of Chicago (2002-2006) BA, Biological Sciences

Graduate:
University of California, Irvine (Fall 2007-Summer 2009) graduate student
University of Washington (Fall 2009-present) graduate student
PhD Candidate (Spring 2011)

Other:
University of Washington (Friday Harbor Labs)
Invertebrate Zoology (Summer 2005)
Biomechanics (Summer 2008)
Fish Biomechanics: Fish 565 (Summer 2010)

Publications:

1. Crofts, S.B. "Finite Element modeling of occlusal variation in durophagous tooth systems" – *Accepted JEB*
2. Sigwart, J. D., Green, P. A. & Crofts, S. B. "Functional morphology in chitons (Mollusca, Polyplacophora): influences of environment and ocean acidification" – *submitted Marine Biology*
3. Kolmann, M.A, Crofts, S.B., Lovejoy, N.R. & Summers, A.P. "The effect of jaw curvature on crushing performance in durophagous stingrays" – *in review JEB*
4. Crofts, S.B. & Summers, S. P. "How to best smash a snail – the effect of tooth shape on crushing load" *J. R.Soc. Interface* 11:20131053
5. Grubich, J.R, Huskey, S., Crofts, S., Orti, G. & Porto, J. "Mega-bites: extreme jaw forces of living and extinct piranhas (Serrisalmidae)" *Scientific Reports* 2:1009 (2012)
6. Crofts, S.B. & Summers, A.P. "Swimming in the Sahara" *Nature* 472 (2011):177-178
7. Crofts, A.R., Lhee, S., Crofts, S.B., Cheng, J., Rose, S. "Proton pumping in the bc_1 complex: A new gating mechanism that prevents short circuits." *Biochimica et Biophysica Acta (BBA) - Bioenergetics* 1757.8 (2006): 1019-1034.

Fieldwork:

Dinosaur Science 2007: 2 week paleontological dig in WY
Gobero Dig fall 2006: 5 week archaeological dig in Saharan Niger
Dinosaur Science 2006: 2 week paleontological dig in WY
Fish and Invertebrate Collection (FHL) 2005, 2010-2014

Professional Organizations:

ICVM (2013)
SEB (2013)
ASIH (2011)
AES (2011)
SVP (2011 - 2015)
SICB (2008 - 2015)
Sigma Xi (2009 - 2013)
Gilbert *Ichthyological* Society (2009, 2010)